Deployment of BISON Models of Fuel Restructuring at High Burnup and Related Fission Gas Behavior in UO_2

INL/RPT-24-81422

Nuclear Energy Advanced Modeling and Simulation (NEAMS)

SEPTEMBER 2024

Pierre-Clément A. Simon
Kyle A. Gamble
Arianna Pagani
Ian T. Ferguson
Daniel Schwen
Logan H. Harbour
Larry K. Aagesen
Stephen Novascone

Idaho National Laboratory

Nathan Capps

Oak Ridge National Laboratory

Michael W. D. Cooper
Christopher Matthews
David Andersson

Los Alamos National Laboratory

Battelle Energy Alliance manages INL for the U.S. Department of Energy's Office of Nuclear Energy

INL/RPT-24-81422

Deployment of BISON Models of Fuel Restructuring at High Burnup and Related Fission Gas Behavior in UO_2

Pierre-Clément A. Simon
Kyle A. Gamble
Arianna Pagani
Ian T. Ferguson
Daniel Schwen
Logan H. Harbour
Larry K. Aagesen
Stephen Novascone
Idaho National Laboratory
Nathan Capps
Oak Ridge National Laboratory
Michael W. D. Cooper
Christopher Matthews
David Andersson
Los Alamos National Laboratory

September 2024

Idaho National Laboratory
Computational Mechanics and Materials Department
Idaho Falls, Idaho 83415

http://www.inl.gov

Prepared for the
U.S. Department of Energy
Office of Nuclear Energy
Under DOE Idaho Operations Office
Contract DE-AC07-05ID14517

Page intentionally left blank

ABSTRACT

This milestone report details the advancements made in fiscal year (FY) 2024 under the Nuclear Energy Advanced Modeling and Simulation (NEAMS) program to improve the modeling of fission gas behavior in high burnup (HBu) UO_2 nuclear fuel in the BISON fuel performance code. As nuclear fuel is pushed to higher burnups, significant microstructural changes occur within the fuel, including the formation of a high-burnup structure (HBS) on the pellet rim and a dark zone deeper within the pellet. These regions, characterized by subgrain formation and increased pore densities, have critical implications for fission gas behavior and release, which are not well understood. The modeling capabilities in BISON did not adequately predict these phenomena, leading to an underestimation of fuel restructuring and—potentially—of fission gas release. To address these gaps, this milestone focused on three key objectives: (1) reviewing and assessing simple integrated fission gas release and swelling (Sifgrs)'s capabilities for low burnup fuel, on which high burnup capabilities rely, (2) validating and expanding HBS fission gas modeling capabilities, including investigating mechanisms for fission gas release (FGR) from HBS, and (3) expanding Sifgrs to enable modeling of dark zone formation and its effects on fission gas behavior. These objectives were achieved and are described herein. The achievements of this NEAMS milestone are significant for the industry's goal of burnup extension. The improved predictive modeling capabilities for both low- and high-burnup conditions enhance our understanding of fuel performance under both normal operations and transient scenarios. Although goals were reached, future work is necessary to validate these models against experimental data and quantify their accuracy in different conditions. In parallel, mechanistic modeling efforts should continue to extend and refine these capabilities to increase accuracy while reducing reliance on empirical models. This will ensure robust performance across a broader range of conditions.

ACKNOWLEDGMENTS

This report was authored by a contractor of the U.S. Government under Contract DE-AC07-05ID14517. Accordingly, the U.S. Government retains a non-exclusive, royalty-free license to publish or reproduce the published form of this contribution, or allow others to do so, for U.S. Government purposes. Funding was provided by the Department of Energy NEAMS program.

This research made use of the resources of the High Performance Computing Center at Idaho National Laboratory, which is supported by the Office of Nuclear Energy of the U.S. Department of Energy and the Nuclear Science User Facilities under Contract No. DE-AC07-05ID14517.

The first author also wants to acknowledge Davide Pizzocri and Tommaso Barani for the fruitful discussions related to the modeling and validation of pore evolution in the high burnup structure.

Page intentionally left blank

CONTENTS

FIGURES

TABLES

Page intentionally left blank

ACRONYMS

BWR	boiling water reactor
FFRD	Fuel, Fragmentation, Relocation, and Dispersal
FGR	fission gas release
FY	fiscal year
GB	grain boundary
GBs	grain boundaries
HBS	high-burnup structure
HBu	high burnup
IFPE	International Fuel Performance Experiments
INL	Idaho National Laboratory
LOCA	loss of coolant accident
LWR	light water reactor
NEAMS	Nuclear Energy Advanced Modeling and Simulation
NR	non-restructured
NRC	Nuclear Regulatory Commission
PWR	pressurized water reactor
Sifgrs	simple integrated fission gas release and swelling
tFGR	transient fission gas release
Xe	xenon

Page intentionally left blank

Deployment of BISON Models of Fuel Restructuring at High Burnup and Related Fission Gas Behavior in UO_2

1. INTRODUCTION

The fission of nuclear fuel results in fission products with a fraction of them being noble gases. These noble gases, mostly xenon (Xe) and krypton (Kr), have little solubility in nuclear fuel and remain as fission gases. They diffuse through the fuel matrix and grain boundaries, join or form intra- and inter-granular bubbles, and eventually get released from the fuel into the fuel-cladding gap and rod plenum [20–22].

Fission gas behavior is central to fuel performance because it degrades the rod thermal conductivity and mechanical behavior. The presence of fission gases within the fuel decreases its thermal conductivity and leads to fuel swelling, cracking, and pulverization, which can result in pellet-cladding interactions. Once released, fission gases reduce the thermal conductance in the fuel-cladding gap and increase the rod internal pressure. As burnup increases, fuel microstructure evolves, which impacts fission gas behavior. As utilities aim to extend the lifespan of their fuel by reaching higher burnups, there is a crucial need to understand and quantify fission gas behavior at high burnups. Unfortunately, only limited experimental data is available under these conditions.

Modeling fission gas release is therefore a crucial part of fuel performance codes to support burnup extension. The Sifgrs model is a state-of-the-art fission gas behavior and swelling model implemented in the fuel performance code BISON [1, 20, 23]. It first focused on UO_2 fuel for low-burnups during normal operations and was expanded to transient conditions and other fuel forms such as chromium-doped UO_2 and U_3Si_2 through the NEAMS program.

Sifgrs employs a generally mechanistic approach to simulate fission gas behavior and describes different steps of fission gas transport and eventual release. It offers leading capabilities for intragranular fission gas modeling [20, 24–29], describes intergranular fission gas behavior in the form of lenticular bubbles with coalescence criteria [20, 27], and accounts for diffusional release and burst release due to microcracking of the fuel during temperature transients [30]. To describe all these different phenomena, Sifgrs leverages a mix of empirical, semi-empirical, and mechanistic models—some of them based on atomistic simulations [31, 32]. Note that all these options available—corresponding to different models or parameter values—can be activated and deactivated by users. This makes Sifgrs a very flexible tool for modeling fission gas behavior.

This flexible approach lends itself to accelerated model development and continuous model improvement as more insight is gained on different aspects of the model. Sifgrs, as a part of BISON, contributes to improving our understanding of fuel performance modeling [33].

Sifgrs was first describe in the seminal 2013 paper by Pastore et al. [20] and has extensively grown since then. New models have been added to include more sophisticated and more accurate mechanisms. Recently, Sifgrs has been refactored to become modular and enable rapid expansion of its capabilities to high burnup conditions and to other fuel forms [1].

However, the high burnup (HBu) capabilities in Sifgrs were still nascent, which can be attributed in large part to the lack of mechanistic understanding of HBu fuel performance. As UO_2 fuel is pushed to higher burnups, important microstructural changes happen throughout the fuel. An high-burnup structure (HBS) region forms on the pellet rim, and a dark region forms deeper within the pellet [17, 34]. These regions are characterized by the formation of subgrains and higher pore densities. These changes have important implications for fission gas behavior and accelerated release, which are currently not understood. At the beginning of fiscal year (FY) 2024, the model of HBS formation did not predict the formation of the dark zone,

therefore underestimating fuel restructuring. Moreover, the description of the fission gas behavior during fuel restructuring and fission gas release (FGR) during operation and loss of coolant accident (LOCA) beyond fuel restructuring is very limited.

To address these shortcomings, this milestone aimed to improve HBS capabilities in BISON/Sifgrs by implementing, to the authors' knowledge, a world-first model to describe the microstructural changes happening in the dark zone region and a model for fission gas behavior during fuel restructuration and to investigate mechanisms for FGR from HBS fuel. These objectives were met, and additional work was done to improve Sifgrs. This milestone report describes the progress made during FY 2024. Contributions included (1) a complete review and assessment of Sifgrs's capabilities to model fission gas behavior in non-restructured (i.e., low burnup) fuel (see Section 2), (2) the development of new HBS modeling capabilities, in particular for HBS pore evolution and diffusional release (see Section 3), (3) the development and introduction in Sifgrs of world-first modeling capabilities for dark zone formation and fission gas behavior (see Section 4), and (4) the assessment and validation of some of Sifgrs's capabilities (see Section 5). Section 6 then concludes the report and provides suggestions for future work.

2. REVIEW, ASSESSMENT, AND IMPROVEMENT OF SIFGRS' CAPABILITIES

2.1. Review of Sifgrs for Low-Burnup Application

Last FY (i.e., FY 2023), Sifgrs was entirely refactored to become more modular, contain less code duplication, and flexible to enable extension to high-burnup conditions and other fuel forms [1]. This FY (i.e., FY 2024), Sifgrs was entirely reviewed to ensure that every submodel was properly implemented with the correct modeling parameters, and properly documented. In other words, the structure of Sifgrs was redesigned in FY 2023, and its content was reviewed and corrected in FY 2024 (see https://github.inl.gov/ncrc/bison/milestone/41).

There are several outcomes from this effort:

1. It led to the correction of several mistakes and typos in the implementation of models in Sifgrs. An example is the implementation of the homogeneous intragranular bubble nucleation model, which incorrectly calculated the single atom radius for the expression provided by Eq. (9) from Ref. [27]. None of these typos led to major differences in fission gas behavior predictions, but they did affect them noticeably and can accumulate. This thorough, line-by-line review has therefore significantly improved Sifgrs.
2. It led to an increase in consistency for model parameters used across Sifgrs. For example, several submodels use the atomic co-volume. However, due to the large uncertainty and different assumptions made by different authors about the Xe co-volume, several values were used in different submodels within Sifgrs. This FY, all these parameters were made consistent across Sifgrs, and the values can now be user-defined to accommodate the preferences of different users or facilitate sensitivity analysis.
3. It led to an increase in documentation, both in the code and on the BISON website. Moreover, a review paper is now being written to provide an overall understanding of Sifgrs and its capabilities for low-burnup application. The full content of the paper is not reproduced here to keep the current report focused on novel capability development, but we aim to submit the paper for publication shortly.
4. It led to the identification of gaps in modeling capabilities and/or validation data, which can direct future efforts. These gaps are discussed in the aforementioned manuscript in preparation.
5. It led to further refactoring efforts to consolidate Sifgrs and increase modularity (the goals of refactoring and the method used to complete it are detailed in Ref. [1]). An example of such a refactoring effort for bubble pressure calculations is explained in Section 2.2. As stated in Ref. [1], refactoring efforts should continue with further development as needs and capabilities evolve.

Although this review work does not lead to novel capabilities *per se*, it is central to ensuring that Sifgrs is accurate, well implemented, and documented, and that it is able to effectively expand to HBu conditions and other fuel forms. Hence, all of the developments described in the rest of this report rely on the review effort succinctly described here.

2.2. Implementation of New Capabilities in Sifgrs for Low-Burnup Application

In this section, we highlight two new capabilities added to Sifgrs: (1) the introduction of a new equation of state to calculate bubble pressure and (2) the ability to account for the arrival of vacancies that assist gas

diffusion from the bulk into bubbles.

To introduce a new equation of state to calculate bubble pressure, the bubble pressure calculations in Sifgrs first needed to be centralized. Until now, Sifgrs only used a simplified Van der Waals equation of state with the assumption that both vacancies and atoms contribute to the bubble volume, as was done in Ref. [20]. Since it was the only option, the implications of using these assumptions on bubble volume, radius, and pressure calculations, as well as the number of atoms and vacancies in each bubble, were implicitly made throughout Sifgrs. A refactoring effort centralized these calculations, which enabled the introduction of a recently developed equation of state by Yang et al. [35]. A new Sifgrs option has therefore been added to enable users to select the equation of state they want to use. The effect of the new equation of state has been described in Ref. [36], where it was implemented.

The ability to track the arrival of vacancies that assist gas diffusion from the bulk is another improvement to Sifgrs' capabilities and is described in Refs. [36, 37]. It affects bubble volume and pressure, which then influences the effective diffusivity of fission gases. Moreover, ongoing efforts are focusing on the development of a mechanistic microcracking model to improve the current empirical capabilities first developed by Pastore et al. and Barani et al. [30, 38]. The presence of additional vacancies, along with the new equation of state described above, will greatly influence the upcoming mechanistic microcracking model.

3. HIGH BURNUP STRUCTURE FISSION GAS BEHAVIOR

3.1. Validation of Existing High-Burnup Structure Capabilities

Existing HBS capabilities were described in detail by Ref. [1]. BISON describes HBS formation based on the models from either Lassmann [39] or Barani et al. [2] and then describes the fuel as a mixture of non-restructured (NR) fuel and HBS similar to Ref. [2]. It also accounts for fission gas transfer from the NR fuel to the HBS as HBS formation occurs, and a larger volume fraction of the overall fuel is covered in HBS. It also captures fission gas generation within the HBS matrix and the fission gas diffusion toward the HBS grain boundaries (GBs), where the fission gases reach the HBS pores. The pores are allowed to grow, but their density is maintained constant as a first approximation. More information about the details of the models is provided in Ref. [1].

Simon et al. [1] demonstrated these models but did not validate them. In this report, we validate these models by compare their predictions to experimental data. Figure 1 shows how the HBS formation and grain size evolution models described in Refs. [1, 2] perform as a function of effective burnup when compared to experimental data from Refs. [3–7]. The HBS model adapted from Barani et al. [1, 2] matches well with the experimental data. The grain size predictions are accurate at high burnup once the fuel is mostly restructured and provides a reasonable value for as-fabricated UO_2 grains at very low burnup. During the transition, however, the grain size is slightly overestimated.

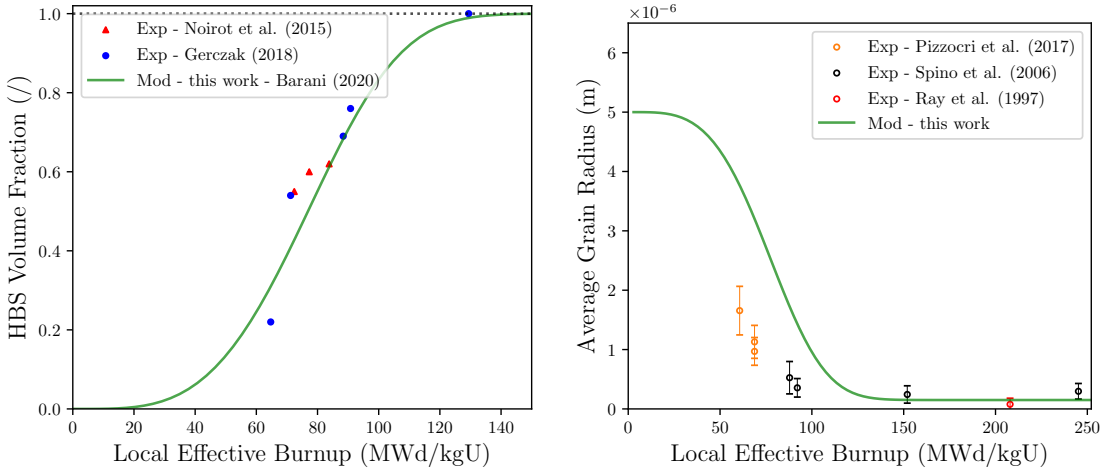

(a) HBS formation.

(b) Grain size evolution.

Figure 1. Validation of the HBS formation and grain size evolution models described in Refs. [1, 2] as a function of effective burnup. Data from Refs. [3–7].

The validation of the fission gas behavior and pore evolution model described in Ref. [1] is shown in Figure 2. The models for Xe concentration in the matrix during HBS formation (both from Lassmann [39] or Barani et al. [2]) perform well. The data shows a large scatter [8–10], but the general trend shows a linear increase as burnup initially increases and a decrease after the effective burnup reaches around 50 to 75 MWd/kgU (i.e., when the HBS forms). The reasons for this decrease is that (1) Xe present in the matrix in NR fuel is captured by GBs during HBS formation and (2) the smaller grains in the HBS shorten the diffusion distance needed for Xe atoms to reach GBs [1]. Once at GBs, fission gases quickly diffuse toward HBS bubbles, which are captured by the model, as shown in Figure 2a. Note that the Xe concentration at the

HBS GBs is null because the HBS grain boundary (GB) diffusivity was assumed to be infinite, meaning that the fission gas would immediately reach the HBS bubbles. This assumption was addressed this FY.

The current pore evolution model, however, does not capture the trends shown by the experimental data [6, 11, 12]. The pore density is assumed to be constant in the model, when measurements show an initial increase in density followed by a decrease past 100 MWd/kgU. The two sources of experimental data (i.e., Refs. [6, 11]) show different magnitudes, but this trend is consistent in both. The pore radius is also not well captured. The order of magnitude is correct, but the pore radius is predicted to stagnate where measurements show a steady increase as burnup increases. The overall swelling due to HBS bubbles is greatly overestimated, which is due to an overestimation of the average radius at burnups ranging from 60 to 150 MWd/kgU, and then an overestimation of the pore density beyond that. These results illustrated a gap in the accuracy of the HBS pore evolution model, which is therefore the focus of the following subsection.

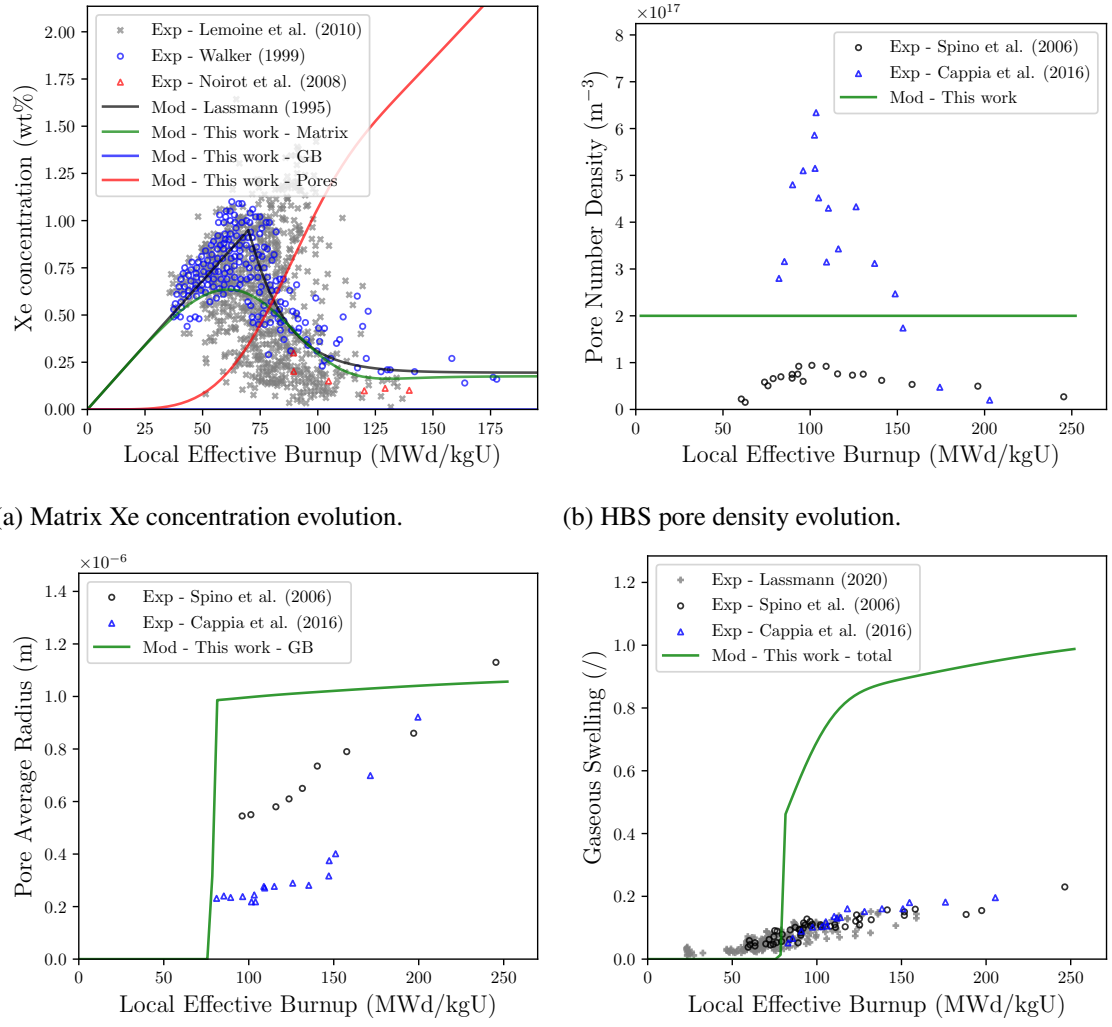

(a) Matrix Xe concentration evolution.

(b) HBS pore density evolution.

(c) HBS pore radius evolution.

(d) HBS pore swelling.

Figure 2. Validation of the HBS fission gas behavior and pore evolution models described in Ref. [1] as a function of effective burnup. Data from Refs. [6, 8–12].

3.2. Development and Implementation of high-burnup structure Pore Evolution Model

3.2.1. A New Pore Evolution Model

The new model builds on the HBS formation model of the previous approach, as well as its fission gas transition model, and its intragranular model [1]. However, the HBS intergranular was revisited to more accurately capture GBs diffusion and HBS pore evolution.

Our first attempt was to implement the mechanistic model described in Ref. [40], but the model predictions were greatly dependent on time step size. Unfortunately, limiting the time step size limits the potential length of overall time that can be modeled. A small time step therefore prevents the effective modeling of high-burnup fuel with an engineering scale fuel performance code such as BISON. More work is therefore needed before this fully mechanistic approach can be reliably applied in BISON.

The approach that we ended up using is therefore a mix between (1) a mechanistic description of HBS pore density to alleviate the previous assumption that the pore density remains constant and (2) an empirical model for HBS pore radius.

The pore density model is from a simplification of the model described in Ref. [40]. It states that

$$\begin{cases} \frac{dN_p}{dt} = \nu_p - bN_p \\ \frac{dC_p}{dt} = 2\nu_p + gN_p - bC_p \\ \frac{dC_{\mathrm{GB}}}{dt} = \kappa - \frac{dC_p}{dt} \end{cases} \tag{1}$$

with N_p the HBS pore number density in m^{-3}, C_p the gas concentration in HBS pores in $\mathrm{mol/m}^3$, C_{GB} the gas single atom concentration HBS GBs in $\mathrm{mol/m}^3$, ν_p the HBS pore nucleation rate in $\mathrm{m}^{-3}\cdot\mathrm{s}^{-1}$, b the resolution rate in s^{-1}, g the trapping rate in s^{-1}, and κ the rate at which gas atoms reach the HBS GBs from the grain bulk in $\mathrm{mol/m}^3\mathrm{/s}$ and is derived from intragranular behavior. The HBS pore nucleation rate ν_p is defined as proportional to the local restructuring rate [40], meaning

$$\nu_p = \nu_p^0 \frac{d\alpha_{\mathrm{HBS}}}{dbu_{eff}^{\mathrm{HBS}}}, \tag{2}$$

with $\nu_p^0 = 1.5 \times 10^{12}$ $\mathrm{MWd\cdot kgU^{-1}\cdot m^{-3}\cdot s^{-1}}$, α_{HBS} the HBS volume fraction, and bu_{eff}^{HBS} the effective burnup for HBS formation [1, 2][1]. Note that the ν_p^0 value was updated from 5×10^{17} in the original paper to better match experimental data [2]. The resolution rate b is from a model proposed by Veshchunov and Tarasov [41]. It defines b as

$$b = b_0 \dot{F} \frac{3d_v}{3d_v + R_P} \frac{\delta}{\delta + R_P}, \tag{3}$$

where $b_0 = 2 \times 10^{-23}$ (-), $d_v = 10^{-9}$ m is the critical distance from the pore surface within which atom resolution occurs, $\delta = 10^{-9}$ m is the thickness of the resolution layer around the pore, and R_p the average HBS pore radius in m. The trapping rate model is originally from Gosële et al. [42]. It states that

$$g = 4\pi D_{\mathrm{GB}}^{\mathrm{HBS}} C_{\mathrm{GB}} R_p \left(1 + 1.8\xi^{1.3}\right) \tag{4}$$

[1]For the derivative of the HBS volume fraction as a function of burnup, we use the version of the model from Ref. [1], which has different model parameters from Refs. [2, 40] to better match experimental data

with D_{GB} the single atom diffusion coefficient in GBs, and

$$\xi = \frac{4\pi}{3} N_p R_p^3 \tag{5}$$

corresponding to the local porosity (/) assuming HBS pores are spherical. The HBS GB diffusivity D_{GB}^{HBS} is not well characterized. However, Olander et al. have determined the GB diffusivity for NR fuel [13], and Barani et al. have proposed a corrective factor for high angle GBs in the HBS [40]. The diffusivity by Olander et al. is equal to

$$D_{GB}^{NR} = 1.3 \times 10^{-7} \exp(-272 \times 10^3 / RT) \tag{6}$$

where T is the temperature in Kelvin and R is the ideal gas constant in J/K/mol. The HBS GBs diffusivity can then be obtained using

$$D_{GB}^{HBS} = D_{GB}^{NR} \frac{\sin\left(4^\circ\left(1-\alpha_{HBS}\right)+40^\circ \alpha_{HBS}\right)}{\sin\left(4^\circ\right)}. \tag{7}$$

As stated above, this approach uses an empirical model to capture the HBS local porosity ξ and drive bubble growth. This model is from the stand alone fission gas behavior SCIANTIX[2]. Based on data from Refs. [6, 11], the HBS local porosity ξ is defined as

$$\frac{d\xi}{dbu} = \xi_0 \tag{8}$$

with $\xi_0 = 3 \times 10^{-4}$ kgU/MWd. The pore radius can then be obtained using Equation (5) assuming spherical pores.

After an increase in HBS pore density and radius, the number density can be reduced by pore interconnection [26]. The pore number density is adjusted as

$$\frac{dN_p}{dV_p} = -4\lambda_p N_p^2, \tag{9}$$

where $\lambda_p = (2-\xi)/(2(1-\xi)^3)$ is a correction factor limiting the interconnection rate when high local porosity is achieved and accounting for the non-superposition of hard spheres [40]. Bubble interconnection also affects the pore radius to ensure that interconnection does not affect the overall pore volume.

While the original model described in Ref. [1] and validated in Figure 2 assumed a constant pore density and used a mechanistic model for pore radius evolution, the new model described above utilizes a mechanistic description of the pore density evolution and an empirical model for porosity and radius calculations. The performances of the two models in reproducing experimental data are tested in the next subsection.

3.2.2. Validation of the New Pore Evolution Model

Figure 3 shows the performance of the new pore evolution model against the same experimental data presented in Figure 2. The match with experimental data is greatly increased compared to the previous approach. The fission gas behavior shown in Figure 3a is only slightly affected with the main change being that a small amount of fission gases is stored at the HBS GBs before HBS pores start to appear around 50 MWd/kgU.

[2]This model was provided by Davide Pizzocri from Politecnico di Milano in private communications and is available on SCIANTIX (see https://github.com/sciantix/sciantix-official/ and Refs.[43, 44]). The same model was utilized as is, but the model parameter ξ_0 was updated.

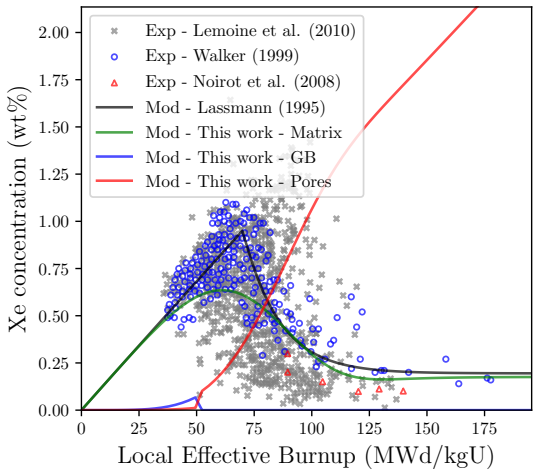

(a) Matrix Xe concentration evolution.

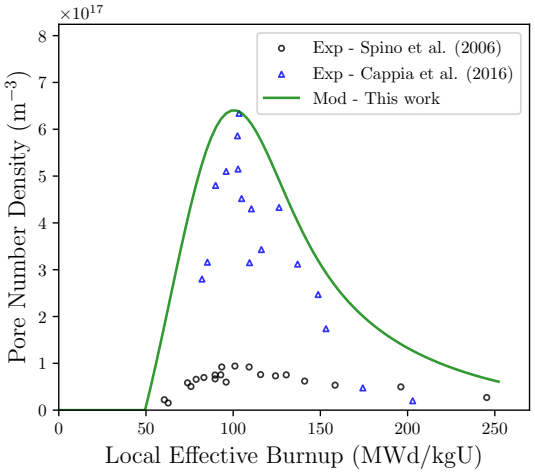

(b) HBS pore density evolution.

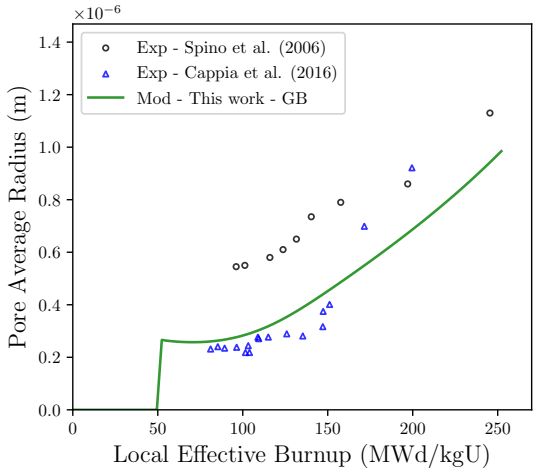

(c) HBS pore radius evolution.

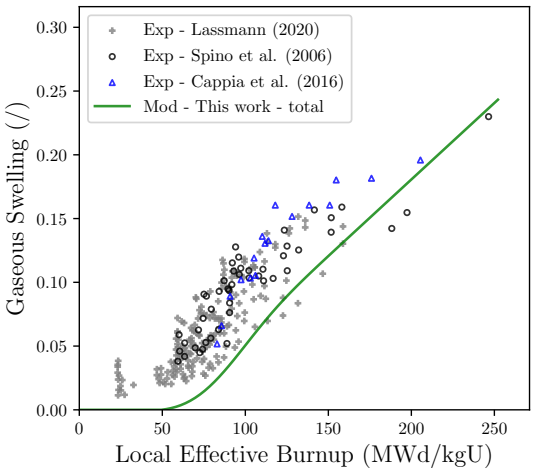

(d) HBS pore swelling.

Figure 3. Validation of the new HBS fission gas behavior and pore evolution models as a function of effective burnup. These results can be compared to those in Figure 2 to show the significant improvement in predicting pore density, pore radius, and swelling. Data from Refs. [6, 8–12].

Concerning pore density, pore radius, and gaseous swelling, however, the performance is remarkably better than the previous models illustrated in Figure 2. Rather than a constant density, the new model captures bubble nucleation, resolution, and interconnection and thus captures the experimental trend (see Figure 3b) (i.e., increasing pore density until around 100 MWd/kgU and then decreasing density due to interconnectivity). The magnitude is also captured, with modeling predictions slightly but consistently overestimating pore density from Ref. [11]. This behavior could be changed by selecting other model's parameters for nucleation and resolution in Equation (3) and Equation (4), but we decided to slightly overpredict density because BISON aims to capture all intergranular pores, including smaller pores that might not be counted during experimental measurements.

Since the swelling data from Ref. [6] was used to impose a swelling rate, it is expected that gaseous swelling, shown in Figure 3d, is accurately captured with model predictions falling within the scatter of the experimental data (albeit slightly low). The HBS pore average radius, dictated by swelling and density,

falls on top of experimental data (see Figure 3c). The accelerated pore growth at higher burnup observed experimentally is now attributed to HBS bubble interconnectivity. These performances are superior to the ones of the previous model presented in Ref. [1] and illustrated in Figure 2, highlighting the importance of properly capturing the pore density evolution, which was assumed to be constant until now. This model, however, is not fully mechanistic since it uses an empirical fit to capture swelling and dictate pore radius evolution. Future work should focus on developing a mechanistic model for pore growth.

3.3. Development of New Diffusional Release Model from high-burnup structure

3.3.1. Modeling Approach

Before this effort, the only mechanism for HBu FGR in Sifgrs was the transient fission gas release (tFGR) resulting from HBS pulverization described in Refs. [1, 45]. There was no capability for diffusional release of fission gases from the HBS, and fission gases accumulated in the HBS structure until pulverization happened. This limitation potentially results in an underestimation of FGR during normal operations at HBu.

To address this limitation, we developed a model for diffusional release of fission gases from HBS GBs. The objective is to estimate the release of fission gas based on the diffusion of gas atoms along grain boundaries. To that end, we aim to provide a semi-analytical expression for the amount of fission gases diffusing out of a domain composed of HBS GBs. In other words, starting with a given amount of fission gas sitting on an HBS GB with a distance δ until a free surface, how much fission gas would be released after a time dt.

Thus, our aim is to solve the diffusion equation:

$$\frac{\partial C_{\mathrm{GB}}}{\partial t} = D_{\mathrm{GB}} \nabla^2 C_{\mathrm{GB}} + S, \tag{10}$$

where C_{GB} (at·m^{-3}) represents the gas concentration at GBs, D_{GB} (m^2·s^{-1}) is the grain boundary diffusion coefficient, and S (at·m^{-3}·s^{-1}) denotes the source term. To simplify the problem, the diffusion is considered on a 1D geometry of length δ, which represents the distance between the initial position of the fission gases and the free surface along GBs. Moreover, in our approach, we neglect the source term and consider, instead, only the initial concentration of gas: $C_{\mathrm{GB}}(t=0) = C_{\mathrm{GB},0}$. This is done assuming that if the diffusion time dt considered is small enough, the inflow of gas atoms that diffuse from within the grain and then reach the grain boundary can be neglected. Note that all the initial fission gas is located at the distance $delta$ from the free surface. Accordingly, we are set to solve:

$$\begin{cases} \frac{\partial C_{\mathrm{GB}}}{\partial t} = D_{\mathrm{GB}} \nabla^2 C_{\mathrm{GB}} & \\ C_{\mathrm{GB}}(x=0, t=0) = C_{\mathrm{GB},0} & \text{I.C.} \\ C_{\mathrm{GB}}(x=\delta, t) = 0 & \text{B.C.} \end{cases} \tag{11}$$

with x the position along the 1D domain (or GB). The boundary condition signifies that the gas concentration is null at the free surface.

The fraction of FGR from the HBS GBs, noted $\mathrm{FGR}_{\mathrm{GB}}$, is then estimated by calculating the overall gas leakage from the start to the end of the diffusion process. This is expressed as one minus the ratio of the gas present in the system at the end of the diffusion process and the initial gas amount, that is

$$\mathrm{FGR}_{\mathrm{GB}}^{\mathrm{HBS}} = 1 - \frac{\int_0^{\delta} C_{\mathrm{GB}}(t = t_{end}) dx}{\int_0^{\delta} C_{\mathrm{GB}}(t = t_0) dx}. \tag{12}$$

The result of this approach depends on three main parameters: (1) the fission gas diffusivity at HBS GB (D_{GB})—the faster diffusion happens, the more release that will occur, (2) the time during which diffusion happens (dt)—the greater the diffusion time, the more release that will occur, and (3) the distance between the initial position and the free surface (δ)—the greater the distance, the lower the release fraction. The goal is to quantify how $\mathrm{FGR}_{\mathrm{GB}}^{\mathrm{HBS}}$ depends on these three parameters to be able to implement this function into Sifgrs to determine diffusional FGR from the HBS region. To that end, we aim to solve Equation (12) on a range of D_{GB}, dt, and δ values and derive a semi-analytical expression. The range of values picked for these three parameters are discussed below.

There is a lot of uncertainty in the value of fission gas diffusivity at HBS GB (D_{GB}), and we attempted to cover a wide range of potential values when developing the semi-analytic expression of $\mathrm{FGR}_{\mathrm{GB}}^{\mathrm{HBS}}$. As described in Section 3.2.1, Sifgrs uses the diffusivity coefficient from Olander and Van Uffelen [13], which is meant for NR GBs, with a correction factor from Barani et al. to adapt it to the high angle HBS GBs [40] (which ranges between 1 and 19.2). To increase the range of diffusivity values accounting for the large uncertainty, we also considered the value from Govers et al. based on molecular dynamics simulations [14]. The diffusivity from Ref. [13] is

$$D_{\mathrm{GB},1} = 1.3 \times 10^{-7} \exp\left(- \frac{4.52 \times 10^{-19}}{k_B T} \right), \tag{13}$$

where k_B (J K^{-1}) is the Boltzman constant, and the diffusivity from Ref. [14] is

$$D_{\mathrm{GB},2} = 3.5 \times 10^{-9} \exp\left(- \frac{1.12 \times 10^{-19}}{k_B T} \right). \tag{14}$$

Figure 4 compares the values of grain boundary diffusivity resulting from the two aforementioned models, evaluating them over a temperature range spanning from 300 K to 1000 K, which aligns well with HBu applications, providing a substantial range of values. For further comparison, values for the intrinsic bulk intra-granular diffusion of fission gas, as formulated by Davies and Long [15] and referred to as D_1 by Turnbull et al. [16], are also included.

As noted, the model by Olander and Van Uffelen yields significantly lower diffusivity values compared to the model by Govers, though still higher than bulk diffusivity. The reason for this lies in the fact that Olander and Van Uffelen aimed to explain the relative immobility—with respect to other fission products—of Xe in UO_2 grain boundaries. Their approach is supported by the exclusion of grain boundary diffusion as a significant mechanism in most fission-gas models [46–51], as well as by microscopic observations of irradiated fuels [52–55]. In contrast, Govers and coworkers proposed a model with much higher diffusivity values [56, 57]. This range of values will dictate the range used in our approach. Note that, in this study, we neglect the effects of traps and pores, considering only pure free diffusion at GBs.

The second parameter influencing $\mathrm{FGR}_{\mathrm{GB}}^{\mathrm{HBS}}$ is the diffusion time dt. In order to be aligned with typical time-step sizes in BISON for diffusional FGR estimations, this quantity was set to range from 1 to 10^6 s. Once implemented in BISON, this parameter will be imposed as equal to the time step.

The third and last parameter to consider is the distance to the free surface δ. The range of δ values should range from a small HBS feature to the longest GB path to a free surface inside the HBS region. Empirical measurements for the rim thickness can be found in the open literature, expressed as a function of either the pellet-edge burnup or the average burnup [58–60]. From these experimental findings, the range for the considered diffusion length has been set to span from 40 to 1400 μm. The upper limit, which is relatively high, aims to also capture the fact that the GB path is tortuous and might be longer than the HBS thickness. Table 1 summarizes the features considered and their respective ranges.

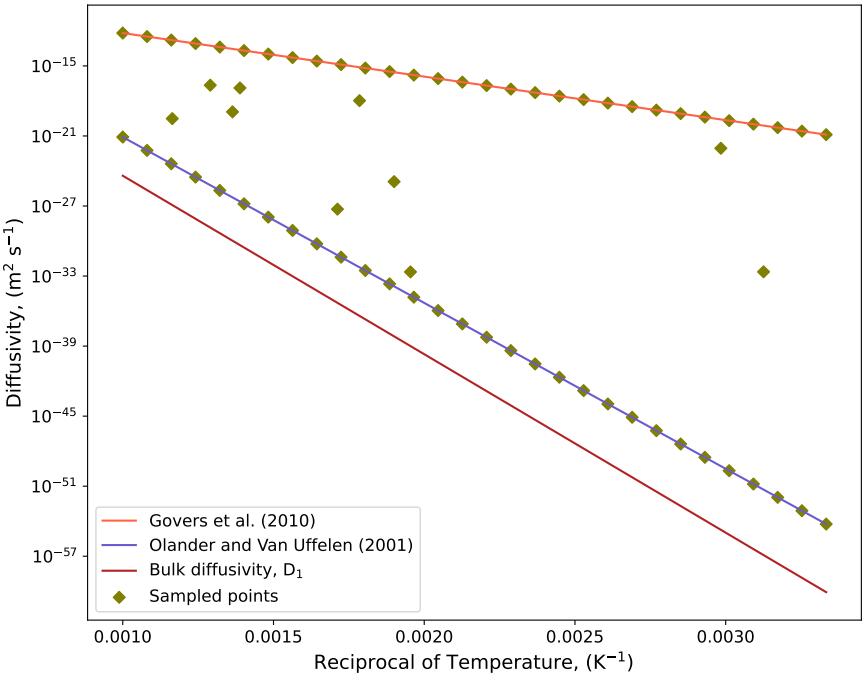

Figure 4. Comparison between the grain boundary diffusivities from Olander and Van Uffelen [13] and Govers et al. [14], further juxtaposed to an estimation of the intrinsic intragranular diffusivity [15, 16].

Table 1. Range of the parameters affecting the solution of Equation (11) and Equation (12).

$\delta(\mu\text{m})$	T (K)	D_{GB} (m^2·s^{-1})	dt (s)
40 – 1400	300 – 1000	$10^{-55} - 10^{-13}$	$10^{0} - 10^{6}$

3.3.2. Numerical Results

Equation (11) was solved numerically 80,000 times over the ranges provided in Table 1. The number of samples drawn from δ, D_{GB} and dt is 40, 50 and 40, respectively. Considering the wide range across with the diffusivity spans, it was decided to sample this parameter more times to better characterize its influence on $\text{FGR}_{\text{GB}}^{\text{HBS}}$. Results are consistent with expectations.

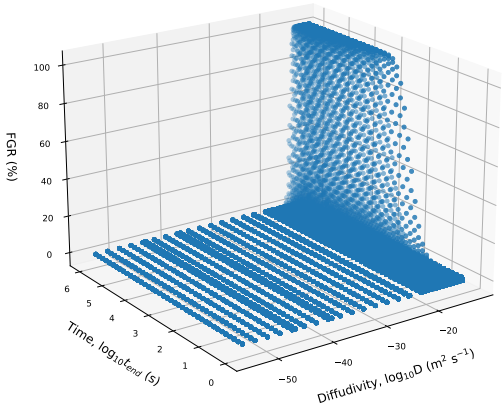

(a) FGR plotted against diffusivity and end time.

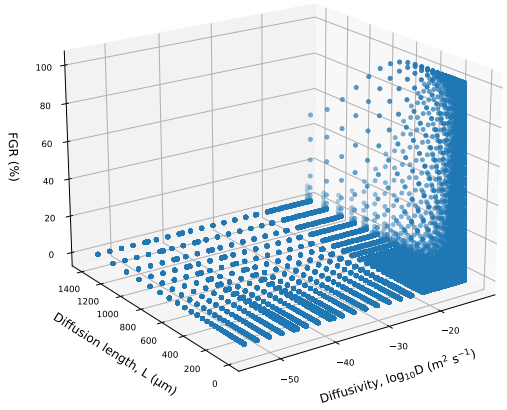

(b) FGR plotted against diffusivity and diffusion length.

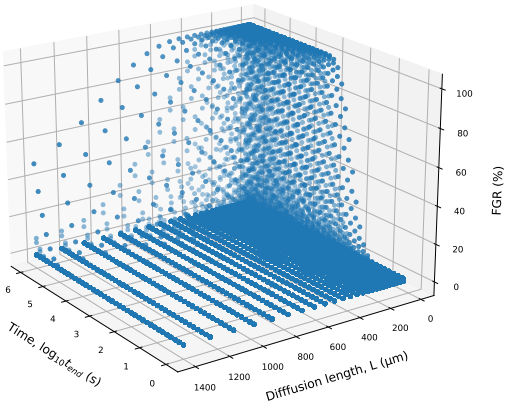

(c) FGR plotted against diffusion length and end time.

Figure 5. Predicted HBS intergranular FGR, resulting from the numerical solution of Equation (11).

In Figure 5, the computed $\mathrm{FGR}_{\mathrm{GB}}^{\mathrm{HBS}}$ values are presented with respect to the aforementioned parameters. Figure 5a shows that $\mathrm{FGR}_{\mathrm{GB}}^{\mathrm{HBS}}$ remains consistently small and close to zero throughout the vast majority of the $\{D_{\mathrm{GB}}, dt\}$ space. An exception to this general pattern exists only at very high diffusivity levels. Once D_{GB} reaches values of approximately 10^{-18} m^2 s^{-1}, regardless of the end time, the onset of a steep release can be observed. For high diffusivity values, if the end time is exceptionally low ($dt \leq 10^2$ s), no release will occur. However as soon as a transition threshold around 10^2 s is reached, the expected $\mathrm{FGR}_{\mathrm{GB}}^{\mathrm{HBS}}$ occurring from diffusion at GBs abruptly increases, rapidly saturating at 100%.

A similar observation can be made for Figure 5b. Across most of the $\{D_{\mathrm{GB}}, \delta\}$ space, $\mathrm{FGR}_{\mathrm{GB}}^{\mathrm{HBS}}$ is practically null, with the sole exclusion of high diffusivity levels ($\approx 10^{-18}$ m^2 s^{-1}). For high D_{GB} values, $\mathrm{FGR}_{\mathrm{GB}}^{\mathrm{HBS}}$ jumps to values as high as 100%, peaking for small values of the diffusion distance and smoothly decreasing as δ grows.

Figure 5c depicts a progression of $\mathrm{FGR}_{\mathrm{GB}}^{\mathrm{HBS}}$ coherent with the observations on the influence of time and diffusion length made above. Once again, the $\{dt, \delta\}$ space is characterized by mostly flat and null values of

release, apart from a zone of maximum FGR_{GB}^{HBS} located at high dt and high δ values.

This trend of increase in FGR_{GB}^{HBS} with respect to the triplet of features considered is intuitive. Diffusivity measures of how quickly atoms move through a medium; therefore, higher diffusivity enhances their motion, increasing the probability of leakage out of the system. It must be noted, however, that the higher values of diffusivity mentioned earlier, for which this pattern is observed, are only compatible with the formulation proposed by Govers et al. for the diffusion coefficient, Equation (14). Additionally, extending the time given for gas atoms to diffuse also induces an increase in FGR. Last, if the characteristic dimension of the system, equivalent to the diffusion length, is small, the probability of leakage will be higher.

3.3.3. A New Model for Diffusional Release from HBS

From the results obtained, our objective is to develop a predictive model for FGR_{GB}^{HBS} as a function of the variables D_{GB}, δ, and dt, such that

$$FGR_{GB}^{HBS} = f(D_{GB}, \delta, dt). \tag{15}$$

After some preliminary analysis, it was found that the impact of D_{GB}, δ, and dt was very interconnected and they could be merged into one dimensionless parameter λ, defined as

$$\lambda = \frac{D_{GB} dt}{\delta^2}. \tag{16}$$

Here, λ (-) can be interpreted as an effective diffusion parameter that encapsulates the interplay between diffusivity, diffusion length, and tim (i.e., the larger the value of λ, the more enhanced the diffusion process). This dimensionless parameter simplifies our task as it effectively combines the key variables governing the diffusion process into a single quantity. Thus, Equation (15) can be rewritten as

$$FGR_{GB}^{HBS} = f(\lambda). \tag{17}$$

The data presented in Section 3.3.2 can be fitted with f defined as a hyperbolic tangent function. For the sake of convenience, the fit was built employing $\lambda^* = \log_{10}(\lambda)$. FGR_{GB}^{HBS} can hence be derived as

$$FGR_{GB}^{HBS}(\lambda^*) = a \tanh[b(\lambda^* s - c)] + d, \tag{18}$$

where a, b, c and d represent, respectively, the amplitude, the steepness, the horizontal shift, and the vertical shift of the hyperbolic tangent and have been determined through regression analysis of the simulation results. Their values are reported in Table 2.

Table 2. Result of the fit to determine the parameters in Equation (18).

a	b	c	d
0.5	2.36454667	-0.42233192	0.5

To rigorously evaluate the performance of the developed fitting model, the coefficient of determination (R^2) was computed. This metric provides a measure of how well the predicted values align with the data. The coefficient of determination is given by

$$R^2 = 1 - \frac{\sum_i (f_i - \hat{f}_i)^2}{\sum_i (f_i - \overline{f})^2}, \tag{19}$$

where:

- f_i represents the actual values of $\mathrm{FGR}_{\mathrm{GB}}^{\mathrm{HBS}}$ obtained from the numerical solution of Equation (11)
- $\hat{f}_i$ denotes the values of $\mathrm{FGR}_{\mathrm{GB}}^{\mathrm{HBS}}$ predicted by the fitted model, Equation (18))
- $\overline{f}$ is the mean of the actual values of $\mathrm{FGR}_{\mathrm{GB}}^{\mathrm{HBS}}$.

The computed R^2 value of 0.999714 indicates an exceptional agreement between the numerical solution and our predictive model. An R^2 value so close to unity not only underscores the robustness of our fitting approach but also validates the effectiveness of using the dimensionless parameter λ in simplifying and accurately modeling the diffusion behavior. The comparison between the $\mathrm{FGR}_{\mathrm{GB}}^{\mathrm{HBS}}$ estimated from the numerical solution of Equation (11) and the fit developed are presented in Figure 6. Furthermore, a closeup of Figure 6a and Figure 6b is depicted in Figure 7 to provide more clarity about the comparison in the non-null $\mathrm{FGR}_{\mathrm{GB}}^{\mathrm{HBS}}$ region.

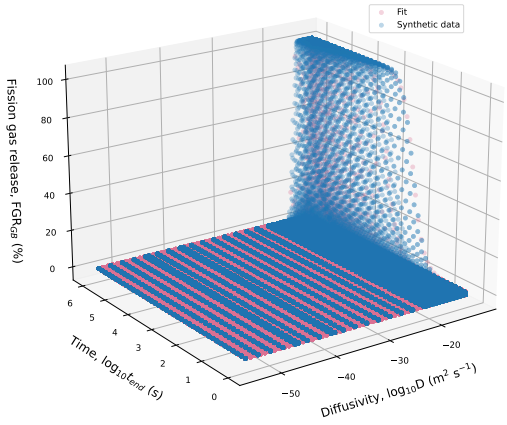

(a) FGR plotted against diffusivity and end time.

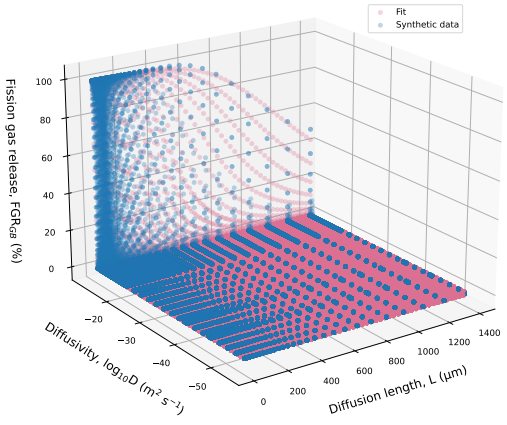

(b) FGR plotted against diffusivity and diffusion length.

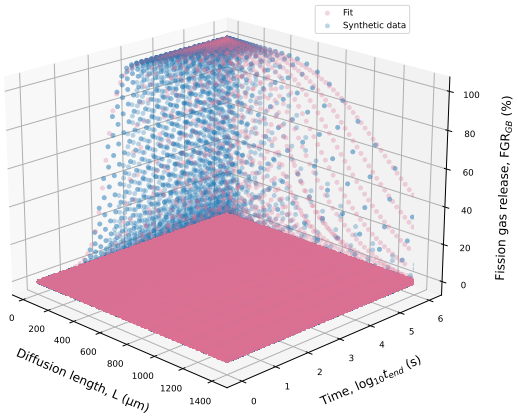

(c) FGR plotted against diffusion length and end time.

Figure 6. Comparison between the HBS intergranular fission gas release resulting from the numerical solution of Equation (11) and the estimates predicted by the fit in Equation (18).

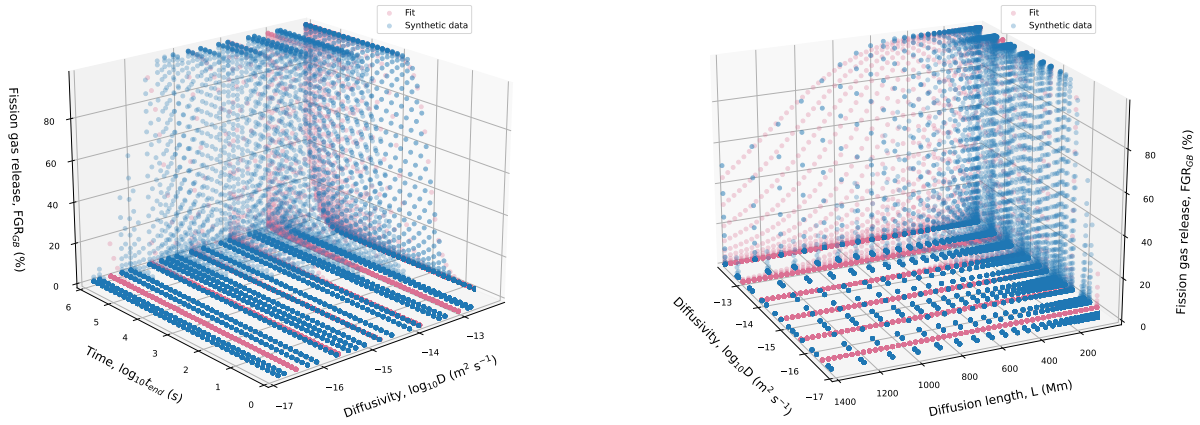

(a) FGR plotted against diffusivity and end time.

(b) FGR plotted against diffusivity and diffusion length.

Figure 7. Close up of the comparison between the HBS intergranular fission gas release resulting from the numerical solution of Equation (11) and the estimates predicted by the fit in Equation (18).

3.3.4. Applicability to Sifgrs or Other Fuel Performance Codes

Equation (18) can easily be implemented in BISON or other fuel performance codes to capture the fraction of fission gas being release through HBS GB diffusion based on the HBS GB diffusivity (i.e., temperature), the time step in BISON, and the distance to the free surface δ. Defining δ is a challenge since the distance to free surface depends not only on the position within the fuel but also on the presence of cracks, pulverized fuel, etc. But a reasonable value within the range provided in Table 1 can be selected as an average until a more sophisticated model is developed.

4. DARK ZONE FORMATION AND IMPACT ON FISSION GAS BEHAVIOR

The presence of a dark zone has been observed by Refs. [17, 34] in high-burnup samples, usually toward the center of the pellet, as opposed to the HBS which is observed at the rim. The dark zone corresponds to significant microstructural changes with an increase in pores and important subgrain formation. These microstructural changes significantly affect fuel performance at high burnup [17, 34], which is why it is key to capture the dark zone in engineering scale codes like BISON. In terms of fission gas behavior, the formation of subgrains, higher pore density, and higher likelihood of cracking and pulverizing during transient conditions [17] is expected to affect FGR in both normal operation and transient conditions. However, to the author's knowledge, no fuel performance code yet captures dark zone formation and the subsequent impact on fission gas behavior. This section hence describes the first attempt at capturing these phenomena.

4.1. Modeling of Dark Zone Formation

The mechanisms for dark zone formation are still unknown. Several hypotheses exist and are being investigated using lower length scale modeling within the NEAMS program, but no clear mechanism has yet emerged. In the meantime, we propose a highly simplistic and speculative model to initiate development. Thanks to Sifgrs's flexibility and modularity, this model can easily be updated or complemented later on as we gain a better understanding of the underlying mechanisms of dark zone formation.

This preliminary model is based on two important observations: dark zone formation occurs (1) at higher burnup ($bu > 50$ MWd/kgU) and (2) in a specific region of the fuel that roughly corresponds to temperatures around 900 and 1100°C. To capture these experimental observations, we adapted the approach first introduced by Barani et al. in Ref. [2] to model HBS formation, which states that fuel restructuring can be captured by a JMAK formulation as a function of effective burnup [2, 61]. The restructured volume fraction for the dark zone, is therefore described as

$$\alpha_{\mathrm{DZ}} = 1 - \exp\left(-Kbu_{eff}^{\gamma_{\mathrm{DZ}}}\right), \tag{20}$$

where the definition of K, bu_{eff} and γ_{DZ} must be adapted to the dark zone.

Because the dark zone seems to appear in a temperature range of around 900 and 1100°C, the definition of the effective burnup bu_{eff} has been updated from Refs. [2, 62] to accumulate only between 900 and 1100°C (as opposed to any temperature below 1000°C). The local effective burnup for dark zone formation is hence defined as

$$bu_{eff} = \int f(T - \bar{T}_{low}) f(\bar{T}_{high} - T) dbu, \tag{21}$$

where f is the Heaviside step function, T is the local temperature in Kelvin, and $\bar{T}_{low} = 900°\mathrm{C} = 1173.15\mathrm{K}$ and $\bar{T}_{high} = 1100°\mathrm{C} = 1373.15\mathrm{K}$ are the threshold temperatures in Kelvin.

The coefficients K and γ_{DZ} from Equation (20) are defined so that dark zone formation occurs at relatively low burnup compared to HBS formation (i.e., around a local burnup of 50 MWd/kgU). They are therefore defined as $K = 1.52 \times 10^{-7}$ (-) and $\gamma_{\mathrm{DZ}} = 4.2$ (-). Note that this model and these values represent a simplistic approach to modeling dark zone formation, and more data and work are needed to improve predictive capabilities. This model is, however, the only one available and will be used in the rest of this report.

The dark zone grains are assumed to have a constant radius of 150 nm, which therefore affects the average grain size during dark zone formation. Figure 8 shows how this model predicts dark zone formation and grain size evolution as the dark zone-effective burnup increases; see Equation (20). When comparing to HBS formation in Figure 1, we can see that dark zone formation happens at a lower burnup. This is by design, as

the HBS forms on the rim region where the local burnup is much higher than deeper in the pellet, where the dark zone is observed.

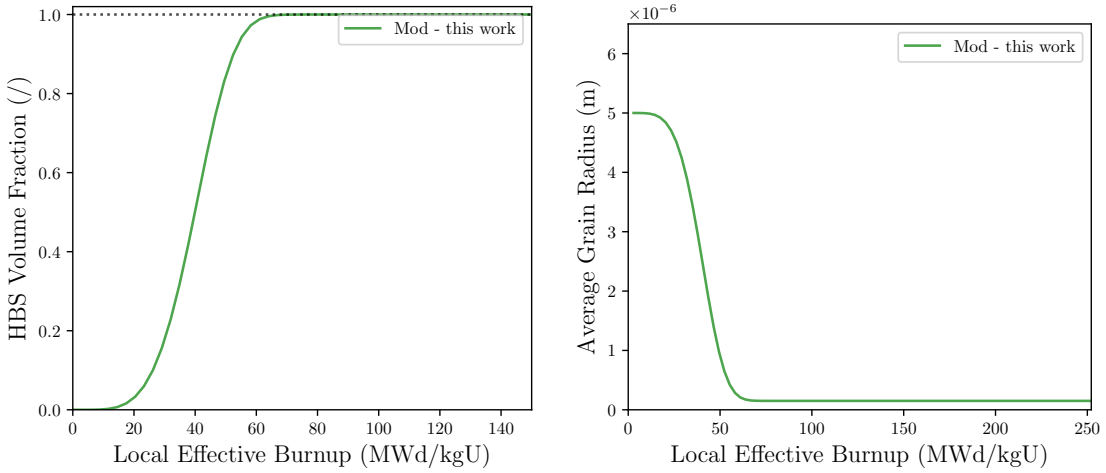

(a) Dark zone formation.

(b) Grain size evolution.

Figure 8. Demonstration of the dark zone formation and grain size evolution models as a function of effective burnup.

Figure 9 demonstrates how the HBS and dark zone formation models predict restructuring along a pellet radius at the end of life of a hypothetical fuel under the constant temperature profile shown in Figure 9a and a constant linear heat rate until the burnup profile shown in Figure 9b is reached. Figure 9c shows how the HBS structure is predicted on the outer edge while dark zone formation is predicted deeper in the cladding, corresponding qualitatively to the experimental observations made in Ref. [17]. The rim region shows high HBS volume fraction. Going inside of the pellet, the HBS volume fraction decreases until a sharp stop around $r/r_0 = 0.4$ due to the 1000°C limit for the HBS effective burnup. The dark zone is observed between $r/r_0 = 0.18$ and $r/r_0 = 0.6$ due to the temperature profile alignment with the temperature range considered when determining dark zone formation; see Equation (20). Toward the center of the pellet, no restructuring is observed due to higher temperatures. Future work should focus on quantitatively validating these restructuring models and guiding future modeling improvements. The dark zone formation model presented herein is preliminary and does not aim to capture the complex mechanisms governing dark zone formation. Future work should focus on developing a more descriptive model.

4.2. A Three-Phase Model for the Non-Restructured Region, HBS, and the Dark Zone

In Barani et al. [2], the fuel is modeled as a two-phase system, with the fuel being part non-restructured and part HBS. This approach is used in Sifgrs as well [1]. However, now that we also model the dark zone, we extend this approach to three phases. Fission gas concentration is therefore shared between the three phases with

$$c^{tot} = (1 - \alpha_{\text{HBS}} - \alpha_{\text{DZ}})c^{\text{NR}} + \alpha_{\text{HBS}}c^{\text{HBS}} + \alpha_{\text{DZ}}c^{\text{DZ}}, \tag{22}$$

where c^{tot} (mol/m^3) is the local fission gas concentration, c^{NR} (mol/m^3), c^{HBS}, and c^{DZ} (mol/m^3) are the local fission gas concentration in the NR, HBS, and dark zone phases, respectively. α_{HBS} and α_{DZ} are the

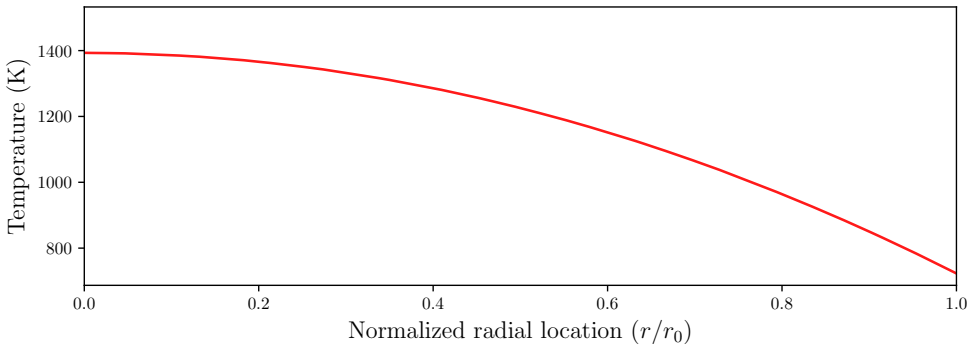

(a) Temperature profile.

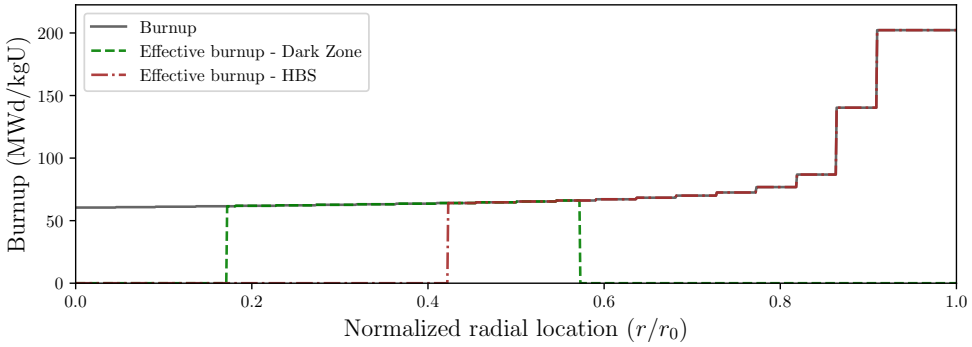

(b) Burnup and effective burnups profiles.

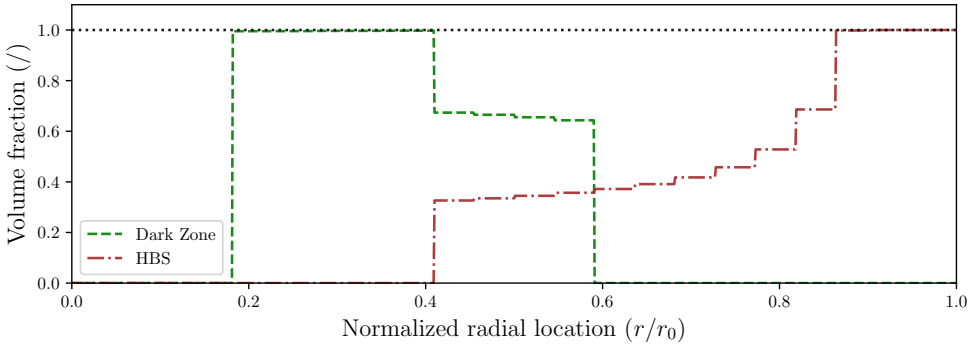

(c) Volume fractions profiles

Figure 9. Demonstration of the HBS and dark zone formation models along a pellet radius during a hypothetical irradiation history. The predictions qualitatively correspond to experimental observations published in Ref. [17]. The steps in the burnup and volume fraction profiles are due to mesh refinement.

local volume fraction of HBS and dark zone, respectively. In the rest of the report, we also use $\alpha_{\mathrm{NR}} = 1 - \alpha_{\mathrm{HBS}} - \alpha_{\mathrm{DZ}}$.

The grain size, bubble populations, dislocation density, and other microstructure parameters of each phase are tracked for each phase and for the complete fuel.

4.3. Modeling of Fission Gas Generation

The amount of fission gas generated is shared between the NR, HBS, and dark zone phases based on their volume fraction, meaning that

$$\beta^{\mathrm{NR}} = \alpha_{\mathrm{NR}}\beta^{tot}, \tag{23}$$

$$\beta^{\mathrm{HBS}} = \alpha_{\mathrm{HBS}}\beta^{tot}, \tag{24}$$

and

$$\beta^{\mathrm{DZ}} = \alpha_{\mathrm{DZ}}\beta^{tot}, \tag{25}$$

where β^{tot} is the local fission gas generation rate density, and β^{NR}, β^{HBS}, and β^{DZ} are the corresponding quantities for each phase.

4.4. Modeling of Fission Gas Transition from the Non-Restructured Region to the Dark Zone

As the fuel transitions to the dark zone, significant microstructural changes happen. These transformations result in noteworthy changes in the location of fission gases. As the dark zone forms during irradiation, fission gases are swept from the non-restructured region. As the dark zone volume fraction increases by $\Delta\alpha_{\mathrm{DZ}}$, the amount of fission gas swept from the non-restructured region corresponds to

$$\Delta c^{\mathrm{NR}} = -\frac{\Delta\alpha_{\mathrm{DZ}}}{\alpha_{\mathrm{NR}}} c^{\mathrm{NR}}. \tag{26}$$

In this model, we assume that the generation of fission products has already been accounted for, so mass conservation imposes that the amount of fission gas swept from the non-restructured fuel equals the amount of fission gas added to the dark zone phase. As such,

$$\Delta c^{\mathrm{DZ}} = -\Delta c^{\mathrm{NR}}. \tag{27}$$

4.5. Intragranular Fission Gas Modeling in the Dark Zone

The intragranular fission gas behavior in the dark zone is currently modeled in the same way as in the HBS [1]. Dark zone grains are assumed to have a constant radius of 150 nm [2], and intragranular fission gases are assumed to diffuse toward grain boundaries. The presence of intragranular bubbles and dislocations, which can affect fission gas transport in non-restructured fuel, is neglected. This assumption, however, is reasonable as a first approximation since experimental data show a very limited intragranular bubble density in the dark zone [17]. Dark zone formation is thought to reduce the density of dislocations like HBS formation, and the dark zone microstructure is dominated by large intergranular bubbles rather than intragranular ones. Moreover, the purely diffusional description of intragranular fission gas behavior is widely used in fuel performance codes. Currently, the dark zone intragranular diffusion coefficient is defined as

$$D^{\mathrm{DZ}} = 4.5 \times 10^{-42} \cdot F, \tag{28}$$

which originates from an empirical study [63]. $\cdot F$ is the fission rate in ($\mathrm{m}^{-3}\mathrm{s}^{-1}$), leading to D^{DZ} being defined in m^2/s. This model will be validated in future work.

4.6. Intergranular Fission Gas Modeling in the Dark Zone

Since limited information is available on intergranular fission gas behavior in the dark zone, we applied the same model as available in the HBS in Sifgrs described in Ref. [1]. This model mechanistically describes pore radius evolution but assumes a constant pore density of 2×10^{17} bubbles/m^3 [1]. Note that we did not apply the recently developed HBS pore evolution model described in Section 3.2 because it relies on an empirical description of gaseous swelling, for which we have no data available in the dark zone. However, a similar approach could be applied to the dark zone as more measurements become available.

4.7. Predictions of Dark Zone Formation and Overall Fission Gas Behavior

Figure 10 shows the predictions related to dark zone formation, fission gas behavior, and dark zone pore evolution as the dark-zone-relevant effective burnup increases. Fission gas behavior is similar to HBS behavior (see Figure 2) with fission gases distributed across the matrix, GBs, and the large intergranular pores. The main difference is that because dark zone formation happens at a lower effective burnup (albeit at higher temperatures), these transitions occur sooner. The dark zone pore evolution is, as expected, equivalent to the HBS behavior since the same models have been adopted.

4.8. Summary and Impact

This section presented, to the authors' knowledge, the world-first dark zone modeling capabilities. A simplistic dark zone formation model was developed and implemented, and semi-mechanistic models for fission gas generation and transition from non-restructured fuel to dark zone, intragranular diffusion, and intergranular pore evolution have been expanded from previous HBS capabilities. This rapid extension was made possible by the refactoring work described in Ref. [1], which increased Sifgrs's modularity. These dark zone modeling capabilities now serve as the foundation for future developments aimed at enhancing predictive accuracy as new insights into dark zone fuel performance are gained through experimental campaigns or mechanistic modeling efforts.

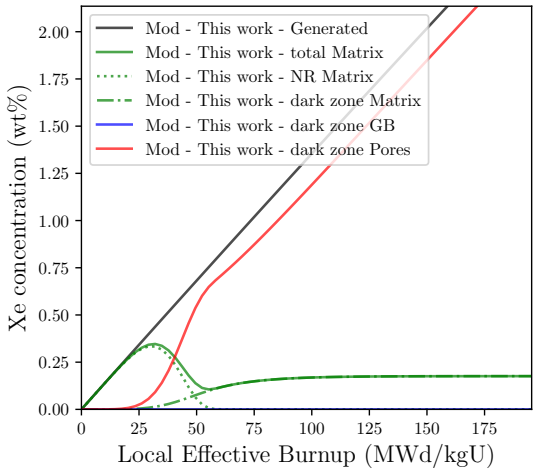

(a) Matrix Xe concentration evolution.

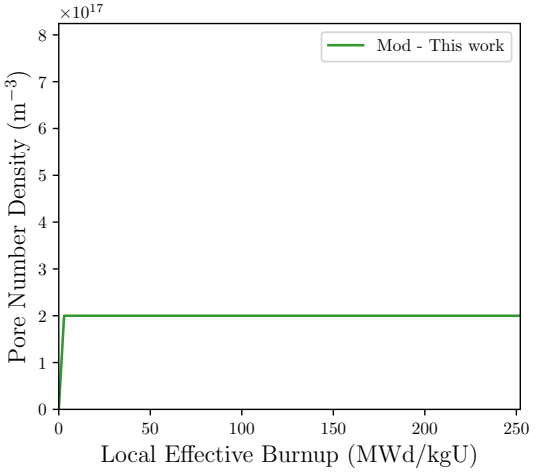

(b) Dark zone pore density evolution.

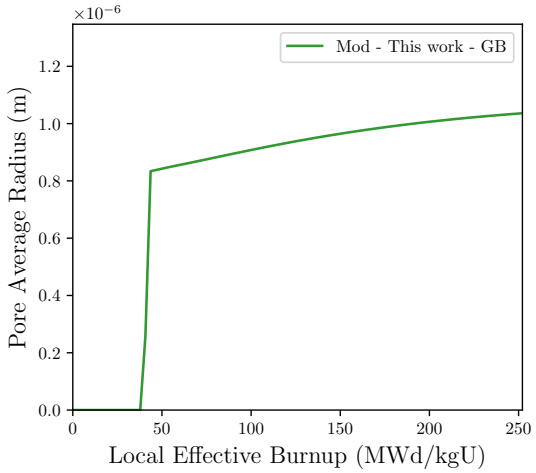

(c) Dark zone pore radius evolution.

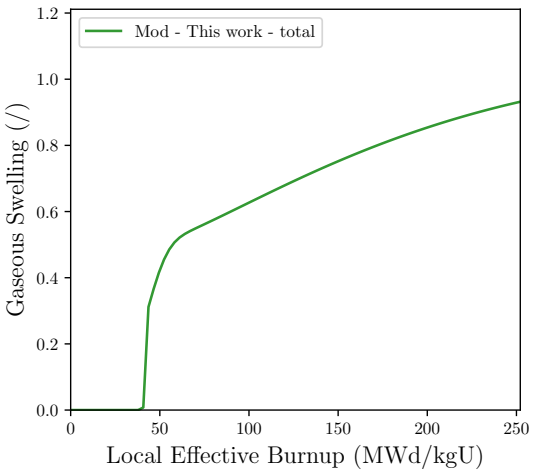

(d) Dark zone pore swelling.

Figure 10. Demonstration of the dark zone fission gas behavior and pore evolution models as a function of effective burnup.

5. ASSESSMENT AND VALIDATION

Assessing and validating Sifgrs is crucial to quantify the accuracy of BISON's modeling capabilities. As such, assessment and validation (1) builds trust in BISON's ability to model fission gas behavior, (2) tracks how accuracy changes as capabilities evolve to quantify the impact of new development, and (3) guide future work when gaps are identified. This section presents concurrent efforts to update, clean up, and template assessment cases in BISON to better assess Sifgrs and its fast-evolving capabilities (see Section 5.1), and assess Sifgrs (see Section 5.2). This effort aims at supporting ongoing and future validation and benchmarking efforts [64–66].

5.1. Updating and Templating Assessment Cases in BISON

BISON contains an large suite of assessment cases with a significant fraction of them having experimental data available for validation. To assess and validate Sifgrs, the assessment cases need to be up-to-date and running. However, since BISON is under continuous development, keeping the assessment cases updated with the latest and brightest models is a challenge. This maintenance task represents a significant effort because each input file potentially needs to be updated with every change in BISON. Moreover, if some input files are missed during updates, some discrepancy can appear between input files that should remain similar. This task, however, could be made much easier by utilizing the recent MOOSE feature of templating input files.

Templating input files consists of consolidating parts of input files that are common within a base input file and having dedicated .i or .params files for each assessment case to list the specific features or parameters used by a specific case. For example, if two assessment cases are identical but use a different temperature history, the base input file would contain all the block and information common to both input files, and the .params files (one for each case) would contain the temperature history. This would prevent having the content of the base class duplicated in two different input files. Maintaining one base input file instead of several duplicate inputs is much more efficient and ensures consistency across similar cases. Moreover, since the case-specific input files now contain only the information specific to that case, it becomes much easier to identify differences between assessment cases. This approach becomes even more effective as the number of cases increase, which since BISON has several dozens of cases, is ideal.

This FY, we initiated an effort to template the assessment cases in BISON. Some of these are still being developed, but some were already merged into BISON (i.e., Seperate_effects_FGB cases). One of these templating efforts for one family of assessment cases lead to a net removal of 7,544 lines across several duplicate inputs, highlighting the large impact this approach has on reducing duplication and associated maintenance needs. This effort also highlighted inconsistencies in assessment cases in the choice of models and modeling parameters, which will help with updating the assessment cases to a unified state consistent with the latest and brightest BISON capabilities.

5.2. Assessment and Validation of Sifgrs

As mentioned previously, BISON has a large suite of inputs to simulate experiments from a wide variety of programs. One of the most common measurements of these experiments is the fission gas release. The focus of this work has been the development and implementation of the dark zone and HBS fission gas behavior models as well as transient fission gas release. Thus, select integral experiment cases have been revisited from the larger BISON assessment suite to investigate current predictive capabilities.

Integral experiments are concerned with obtained measurements of fuel performance metrics under

more prototypical conditions than separate effects experiments. This means several physical phenomena are ongoing at the same time an experiment is capturing the results of the interaction of those phenomena. Here, the Studsvik Super Ramp and Nuclear Regulatory Commission (NRC)–sponsored LOCA simulations are revisited. Another effort not presented here is the first author' participation in the OECD Nuclear Energy Agency (NEA) Expert Group on Reactor Fuel Performance benchmark activity to investigate transient fission gas capabilities on the REGATE and HATAC-C2 cases, which resulted in a submitted paper at the ANS's TopFuel meeting [66].

5.2.1. Super Ramp

The Studsvik Super Ramp project [67] investigated the behavior of typical light water reactor (LWR) test fuel rods when subjected to power ramps after base irradiation to medium burnups. While not applicable for evaluating the HBS developments highlighted in preceding sections of this report, power ramp experiments at any burnup are excellent for evaluating the impact of the transient microcracking models available in Sifgrs. The Super Ramp project contained two subprograms for pressurized water reactor (PWR) and boiling water reactor (BWR). To date, BISON contains inputs to simulate 11 of the 28 rods in the PWR subprogram. These cases correspond to three of the six groups within the subprogram (PK1, PK2, and PK6). The power level and discharge burnup ranges of the commercial rods prior to power ramping are summarized in Table 3.

Table 3. Summary of burnup and linear heat rate ranges of the base irradiation of the 10 rods analyzed from the Super Ramp PWR subgroup. The ranges provided correspond to the radial average values at peak axial location.

Rod Group	Burnup Range (MWd/kgU)	Linear Heat Rate Range (kW/m)
PK1	33–36	19–26
PK2	41–45	17–25
PK6	34–37	20–27

The rods used in the Super Ramp experiments did not undergo refabrication prior to the experiment. Table 4 presents the as-fabricated conditions of the rods.

Table 4. Super ramp rod specifications for the groups analyzed.

Parameter	PK1	PK2	PK6
Rod length (m)	0.388	0.390	0.390
Fuel stack height (m)	0.312	0.318	0.314
Nominal plenum height (m)	0.032	0.032	0.033
Fill gas composition	He	He	He
Fill gas pressure (MPa)	2.25	2.25	2.25
Fuel material	UO_2	UO_2	UO_2
Fuel enrichment (wt.%)	3.2	3.21	2.99
Fuel density (% theoretical)	94.6	94.3	95.1
Fuel outer diameter (mm)	9.11	9.14	9.14
3D grain diameter (μm)	9.36	8.58	34.3
Cladding material	Zirc-4	Zirc-4	Zirc-4
Cladding outer diameter (mm)	10.76	10.75	10.74
Cladding inner diameter (mm)	9.31	9.28	9.29

The power histories that each rod is subjected to include the base irradiation and subsequent ramp test. The rod axial profile, cladding surface temperature, fast neutron flux, and coolant pressure that are applied as provided from the International Fuel Performance Experiments (IFPE) database [68]. For the BISON analyses completed here, a 2D-RZ axisymmetric representation of the rod is assumed. QUAD8 finite elements are used. Compared to the input that is committed to the BISON repository, the only changes made include the addition of the `HighBurnupStructureFormation`, `UO2PulverizationMesoscale`, and `UO2PulverizationTransientFissionGasRelease` models as well modifications to the settings of Sifgrs. These settings are used to activate the most advanced models available in Sifgrs [1]. The new input file block for Sifgrs is shown below:

Listing 1. Sifgrs block for Super Ramp cases

```
[fission_gas_release]
  type = UO2Sifgrs
  block = pellet
  grain_radius = grain_radius
  burnup_function = burnup
  temperature = temperature
  hydrostatic_stress = hydrostatic_stress
  gbs_model = true
  ath_model = true
  hbs_model = true
  hbs_material = High_Burnup_Structure_Formation
  rod_ave_lin_pow = power_history
  ig_bubble_model = NUCLEATION_RESOLUTION
  ig_diff_algorithm = polypole2
  diff_coeff_option = TURNBULL_D1_4D2_D3
  transient_option = MICROCRACKING_BURNUP
  pellet_brittle_zone = pbz
  pellet_id = pellet_id
[]
```

The results of interest from the Super Ramp experiments is the integral fission gas release measurements. Figure 11 presents a measured versus predicted plot of the total fission gas released for the Super Ramp rods analyzed in this work, PK1-1, PK1-2, PK1-3, PK1-4, PK2-1, PK2-3, PK2-4, PK6-2, PK6-3, and PK6-S. The 45° line represents a perfect agreement. The acceptable range of bands correspond to a factor of two as per Pastore et al. [24]. Agreement between BISON and the experimental measurements is good for the PK1 and PK2 series of tests. Comparisons to the large grained fuel in the PK6 group highlights calculated fission gas release values that are lower than the experiment. As grain size increases, the diffusion length of fission gases within the bulk, one of the limiting factor for release, is increased. As expected, the experimental data shows this effect. The modeling predictions, albeit capturing this trend, seem to overestimate the effect of the larger grains on fission gas diffusion and release.

5.2.2. NRC–Sponsored Studsvik Experiments

The NRC-sponsored Studsvik experiments were designed to investigate Fuel, Fragmentation, Relocation, and Dispersal (FFRD) on high burnup fuel rods. The series consisted of six experiments, four of which have been analyzed by BISON. Three of the rods, 191, 192, and 193, were subjected to the same base irradiation

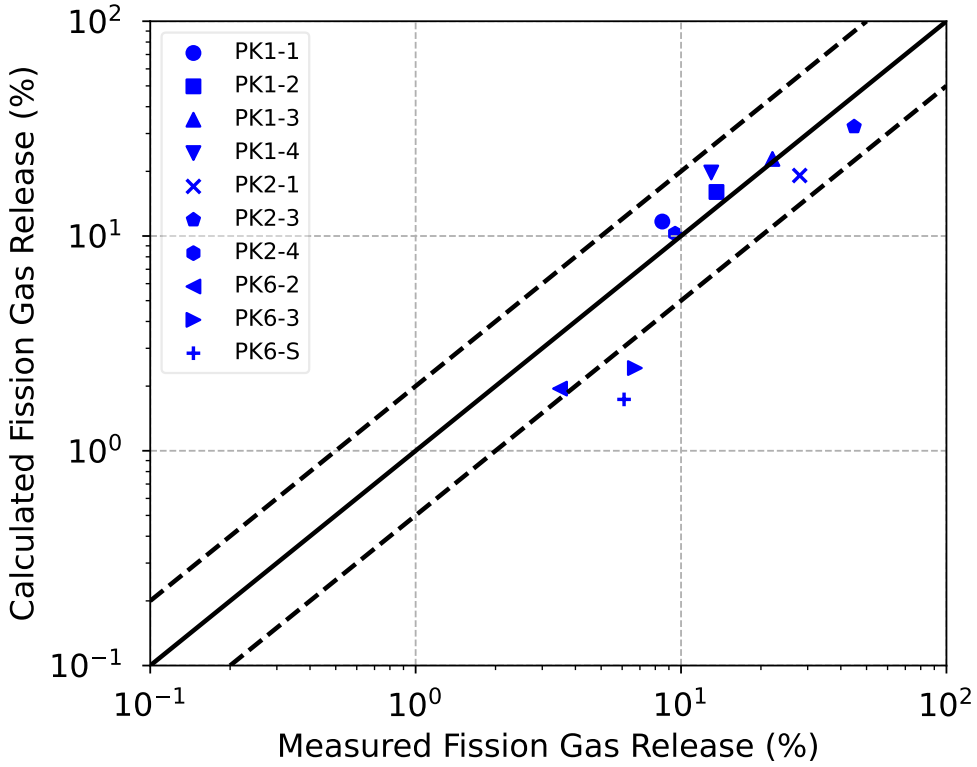

Figure 11. Measured versus predicted plot of fission gas release of the ten rods analyzed with BISON.

history [69]. For Rod 196, it is known two cycles were used to achieve the discharge burnup (∼55 MWd/kgU), but the detailed history is not available. Therefore, a representative two cycle irradiation was assumed as shown in Figure 12a. After the base irradiation, the rodlets were refabricated and inserted into the Studsvik test train inside a hot cell. The experimental specimens are subjected to external heating at a rate of 5 K/s to the target peak cladding temperature. This temperature was 1443 K for Rods 191, 192, and 193 and 1233 K for Rod 196. Figure 12b illustrates the time history of the maximum temperature supplied to the cladding outer surface. This maximum occurs at the rod axial midplane. A slight axial profile on the temperature (20 K less at the ends) is assumed to induce localized ballooning. Table 5 provides additional information related to the four rods. The additional free volume corresponds to the volume outside of the rod but able to communicate directly with the plenum (i.e., the pressure lines).

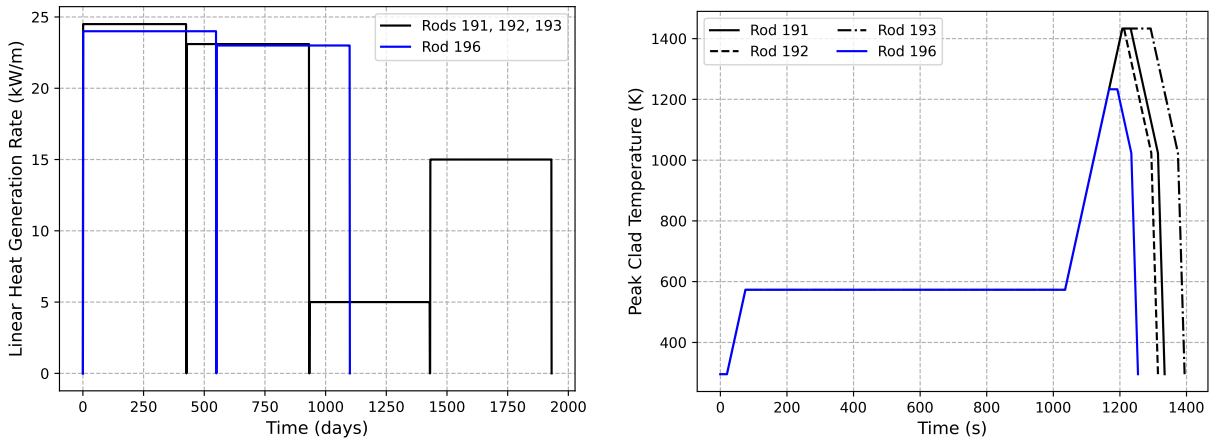

(a) (b)

Figure 12. (a) The linear heat generation rate supplied to the rods during base irradiation and (b) the temperature applied to the cladding outer surface during the experiment.

Table 5. Manufacturing and operational characteristics of Studsvik Rods 191, 192, 193 and 196 [18, 19].

Parameter	**Rod 191**	**Rod 192**	**Rod 193**	**Rod 196**
Rod height (mm)	300	300	300	300
Pellet stack height (mm)	265.4	265.4	265.4	260.6
Pellet radius (mm)	4.1	4.1	4.1	3.92
Gap thickness (mm)	0.08	0.08	0.08	0.08
Cladding thickness (mm)	0.57	0.57	0.57	0.57
Cladding material	ZIRLO	ZIRLO	ZIRLO	ZIRLO
Upper plenum height (mm)	21.86	21.86	21.86	24.86
Lower plenum height (mm)	12.75	12.75	12.75	14.5
Additional plenum volume (cm^3)	8.5	8.5	8.5	8.5
Fill gas (mm)	He	He	He	He
Fill gas pressure (MPa)	2	2	2	2
Refabrication pressure (MPa)	11	8.2	8.2	8.2
IFBA coating	NO	NO	NO	YES
Peak cladding temperature (K)	1433	1433	1433	1233
Time at Peak cladding temperature (s)	25	5	85	N/A

The BISON analyses assume a 2D-RZ axisymmetric geometric representation of the fuel rodlets. The provided base irradiation is supplied to the experimental rodlet dimensions as the full mother rod characteristics are unknown. Furthermore, it is difficult to map data from a full length rod to a segmented rodlet of different dimensions and different mesh density.

The measured results of the Studsvik LOCA tests were primarily concerned with cladding deformation, rod internal pressure, rupture opening characteristics, and fuel dispersal. Of these metrics, the most relevant for evaluating fission gas behavior models is the plenum pressure. A plastic instability failure criterion is assumed in the study here, which assumes failure occurs at an inelastic (i.e., creep) strain rate $\sim 2.7778 \times 10^{-2}$ s^{-1}. Two simulations are completed here: one with the same options active in Sifgrs as used in the Super Ramp simulations and a second where the HBS models are not active in Sifgrs. The amount of fission gases

in different locations is described in Figure 13 for base irradiation for both rods—with and without HBS capabilities. Since Sifgrs tracks the amount of fission gases in the intragranular matrix, intragranular bubbles, intergranular bubbles, and in each equivalent feature in the HBS region, it is possible to understand how each model affects fission gas behavior. The main effect of adding the HBS model is that fission gases are being swept from the NR region and accumulating into the HBS pores. This effect slightly reduces the diffusional FGR, hinting at the fact that current HBS capability might underestimate the release from HBS pores.

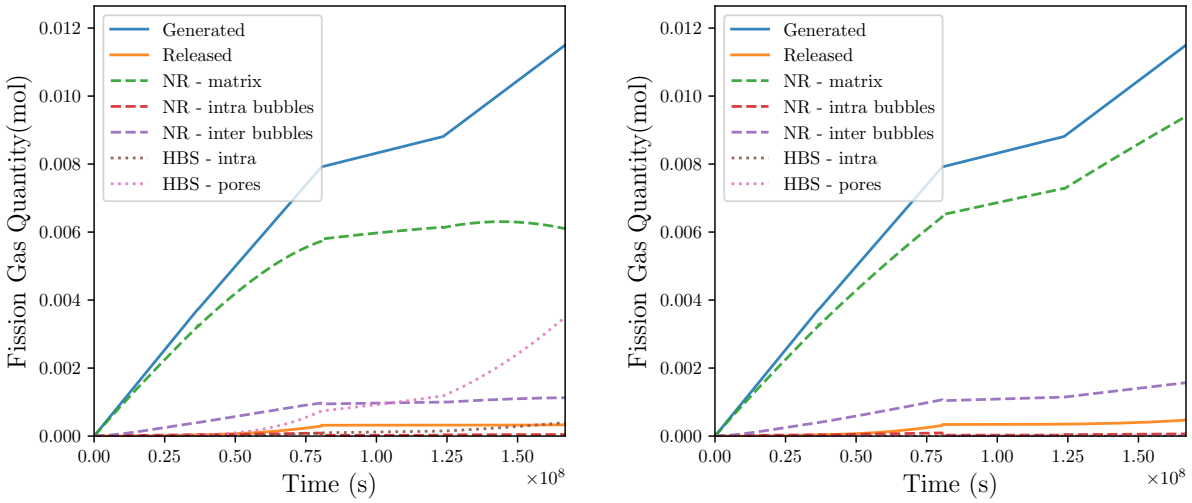

(a) Rod 191 with HBS models

(b) Rod 191 without HBS models

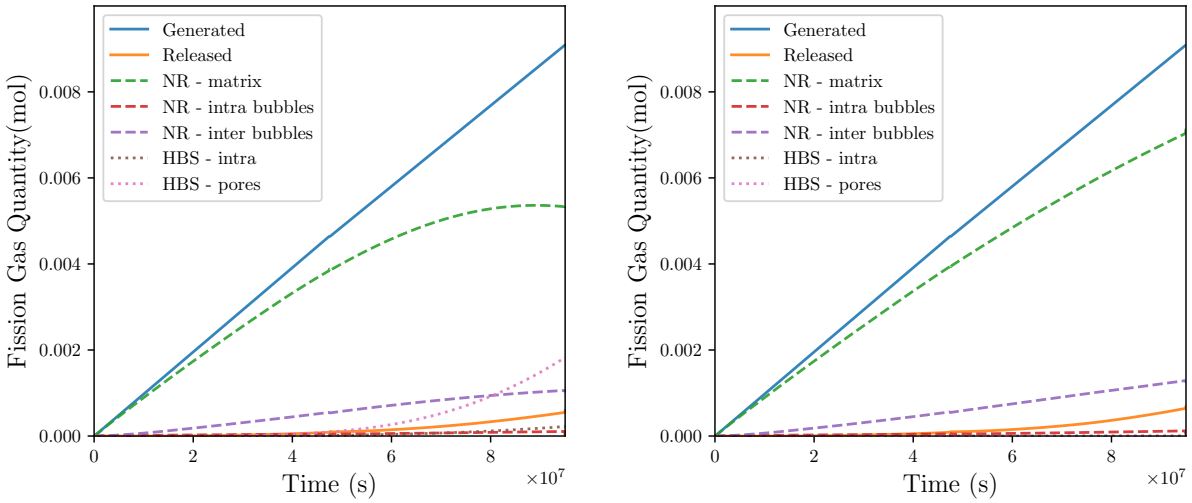

(c) Rod 196 with HBS models

(d) Rod 196 without HBS models

Figure 13. Quantity of fission gas released and stored in various locations within the fuel for (a) Rod 191 when using the HBS models, (b) Rod 191 without HBS models, (c) Rod 196 when using the HBS models, and (d) without HBS models.

The calculated FGR evolution and rod internal pressure for Rods 191 and 196 during the LOCA transient are presented in Figure 14. The time at which the temperature begins to rise from the 553 K shortly after 1000 seconds of conditioning is set to $t = 0$ s. The fission gas curves are reset to zero after the base irradiation to coincide with refabrication. Solid lines correspond to results that including the HBS models and the

dashed lines do not include HBS. The small amount of FGR shown in the results was released during the rise from room temperature up to the condition temperature of 553 K. During the temperature rise, no additional transient FGR due to pulverization is predicted. For Rod 196, this is expected behavior due to the burnup being relatively low such that pulverization is not expected. However, Rod 191 is a higher burnup rod, and further tFGR would be expected. The empirical tFGR model from Capps et al. [33] was not included, but Simon et al. [1] illustrated that this empirical model predicted a large amount of tFGR for Studsvik Rod 191. This discrepancy should be investigated in future work. The difference in calculated rupture time is about the same between the two cases for both Rod 191 and 196. A slightly higher plenum pressure is computed for the case with the HBS models prior to the temperature ramp initiating. These assessments form the basis to evaluate, quantify, and guide future developments.

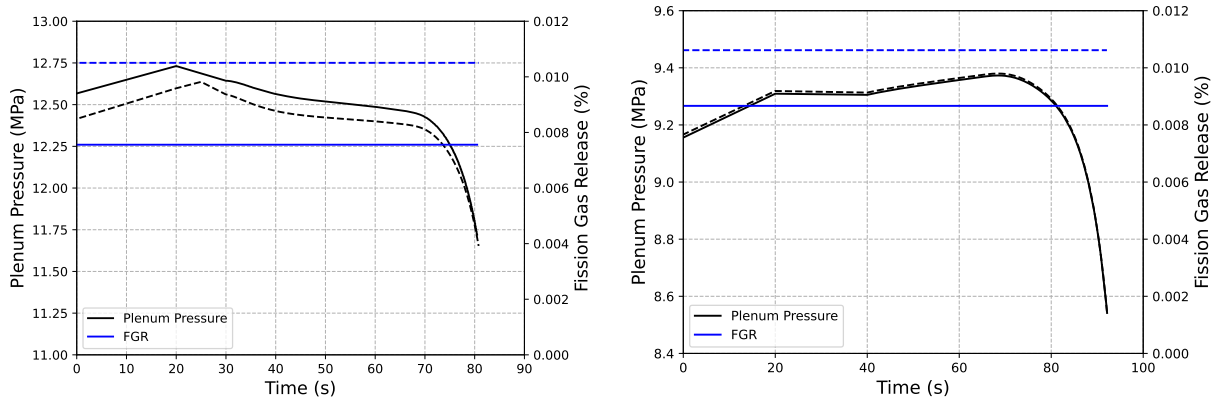

(a) Rod 191

(b) Rod 196

Figure 14. Fission gas release and plenum pressure evolution during the heating phase of the transient for (a) Rod 191 and (b) Rod 196. Solid lines include the HBS models, and dashed lines neglect HBS.

6. CONCLUSION AND FUTURE WORK

The modeling effort presented in this report aims to support the industry's goal to extend fuel utilization by reaching higher burnups. To ensure that fuel performance is maintained within acceptable limits, it is crucial to better understand and quantify fission gas behavior, as it directly affects the rod's thermal conductivity and mechanical behavior. This milestone described the work funded by the NEAMS program in FY 2024 to support burnup extension in improving and extending the fission gas behavior modeling capabilities in the fuel performance code BISON.

The work centered around four main tasks:

1. A complete review and assessment of Sifgrs's capabilities to model fission gas behavior in non-restructured (i.e., low burnup) fuel. This effort was key to ensuring that Sifgrs is reliable, tested, documented, and behaves as expected. It builds strong foundations that the high-burnup capabilities can expand from and depend on. A paper is under preparation to describe and document the current state of Sifgrs for low burnup applications.

2. The development and validation of new HBS modeling capabilities, in particular for HBS pore evolution and diffusional release. The capabilities implemented last year were validated against experimental data, and gaps were identified. The main gap was the inadequacy of the pore evolution model, which did not capture how the pore density evolves as burnup increases, hence inaccurately modeling HBS pore pressure and fuel swelling. This gap was addressed with a new model, which captures these trends with great accuracy. Moreover, another gap was the lack of a diffusional release model for fission gases in HBS, so a new model was developed. These improvements mark a significant leap forward in providing predictive modeling capabilities for burnup extension.

3. Development and introduction in Sifgrs of world-first modeling capabilities for dark zone formation and fission gas behavior. Dark zone formation has been observed experimentally in high-burnup fuel and is expected to significantly affect fuel performance. However, very limited experimental data is available to quantify these effects. As a result, mechanistic modeling approaches have a pivotal role to play in advancing our understanding of high-burnup fuel performance by exploring the new mechanisms activated by the presence of the dark zone. This FY, we implemented—to the authors' knowledge—the first dark zone capabilities. We developed and implemented a preliminary model for dark zone formation and describe how fission gases transition from the NR fuel into the dark zone microstructure. These capabilities were demonstrated on a prototypical fuel simulation. This is a significant first step toward mechanistic modeling of the dark zone's effect on fuel performance at high burnup.

4. The assessment and validation of some of Sifgrs's capabilities. As models are developed, it is crucial to assess and validate them on a variety of relevant cases, including separate effect and integral cases. In this task, we initiate a thorough update and clean up of BISON's assessment cases and applied Sifgrs's capabilities to a few assessment cases. The goal is to build up a list of key assessment and validation cases to continuously monitor how Sifgrs's performance evolves as new models are developed.

The work described in this milestone represents significant advancements in BISON's fission gas behavior modeling capabilities in both low-burnup and high-burnup conditions and both normal operation and transient situations. In particular, the remarkable improvement in modeling HBS pore evolution and the new dark zone modeling capabilities are key breakthroughs in NEAMS's effort to support burnup extension. Future work should include (1) advancing the modeling efforts to improve the current models and reduce reliance on

empirical models by developing mechanistic models that can be extended to a broader range of conditions, (2) developing and implementing new models for fission gas release from the HBS and the dark zone, and (3) thoroughly assessing and validating Sifgrs's capabilities to evaluate its performance and identify gaps to guide future efforts. These necessary efforts have been initiated in a coordinated fashion across several Department of Energy Laboratories and programs, including NEAMS and the Advanced Fuel Campaign.

7. REFERENCES

[1] P.-C. A. Simon, L. K. A. Jr., N. Capps, M. W. D. Cooper, K. A. Gamble, L. H. Harbour, C. Matthews, S. R. Novascone, D. Schwen, and B. Wirth, "Compare predictions of transient fission gas release by empirical and mechanistic models to experiments in high burnup UO_2 fuel," tech. rep., Idaho National Laboratory INL/RPT-23-75026, 9 2023.

[2] T. Barani, D. Pizzocri, F. Cappia, L. Luzzi, G. Pastore, and P. V. Uffelen, "Modeling high burnup structure in oxide fuels for application to fuel performance codes. Part I: High burnup structure formation," *Journal of Nuclear Materials*, vol. 539, p. 152296, 10 2020.

[3] J. Noirot, Y. Pontillon, S. Yagnik, and J. A. Turnbull, "Post-irradiation examinations and high-temperature tests on undoped large-grain UO_2 discs," *Journal of Nuclear Materials*, vol. 462, pp. 77–84, 7 2015.

[4] T. J. Gerczak, C. M. Parish, P. D. Edmondson, C. A. Baldwin, and K. A. Terrani, "Restructuring in high burnup UO_2 studied using modern electron microscopy," *Journal of Nuclear Materials*, vol. 509, pp. 245–259, 10 2018.

[5] D. Pizzocri, F. Cappia, L. Luzzi, G. Pastore, V. V. Rondinella, and P. V. Uffelen, "A semi-empirical model for the formation and depletion of the high burnup structure in uo2," *Journal of Nuclear Materials*, vol. 487, pp. 23–29, 4 2017.

[6] J. Spino, A. D. Stalios, H. S. Cruz, and D. Baron, "Stereological evolution of the rim structure in pwr-fuels at prolonged irradiation: Dependencies with burn-up and temperature," *Journal of Nuclear Materials*, vol. 354, pp. 66–84, 8 2006.

[7] I. L. Ray, H. Matzke, H. A. Thiele, and M. Kinoshita, "An electron microscopy study of the rim structure of a uo2 fuel with a high burnup of 7.9*Journal of Nuclear Materials*, vol. 245, pp. 115–123, 6 1997.

[8] F. Lemoine, D. Baron, and P. Blanpain, "Key parameters for the high burnup structure formation thresholds in oxide fuels," in *Proceedings of 2010 LWR Fuel Performance/TopFuel/WRFPM*, 9 2010.

[9] C. T. Walker, "Assessment of the radial extent and completion of recrystallisation in high burn-up uo2 nuclear fuel by epma," *Journal of Nuclear Materials*, vol. 275, pp. 56–62, 10 1999.

[10] J. Noirot, L. Desgranges, and J. Lamontagne, "Detailed characterisations of high burn-up structures in oxide fuels," *Journal of Nuclear Materials*, vol. 372, pp. 318–339, 1 2008.

[11] F. Cappia, D. Pizzocri, A. Schubert, P. V. Uffelen, G. Paperini, D. Pellottiero, R. Macián-Juan, and V. V. Rondinella, "Critical assessment of the pore size distribution in the rim region of high burnup UO_2 fuels," *Journal of Nuclear Materials*, vol. 480, pp. 138–149, 11 2016.

[12] K. Lassmann and H. Benk, "Numerical algorithms for intragranular fission gas release," *Journal of Nuclear Materials*, vol. 280, pp. 127–135, 7 2000.

[13] D. Olander and P. Van Uffelen, "On the role of grain boundary diffusion in fission gas release," *Journal of Nuclear Materials*, vol. 288, pp. 137–147, 2001.

[14] K. Govers, C. L. Bishop, D. C. Parfitt, S. E. Lemehov, M. Verwerft, and R. W. Grimes, "Molecular dynamics study of Xe bubble re-solution in UO_2," *Journal of Nuclear Materials*, vol. 420, pp. 282–290, 1 2012.

[15] D. Davies and G. Long, "The emission of xenon-133 from lightly irradiated uranium dioxide spheroids and powders," tech. rep., United Kingdom Atomic Energy Authority, 1963.

[16] J. A. Turnbull, C. A. Friskney, J. R. Findlay, F. A. Johnson, and A. J. Walter, "The diffusion coefficients of gaseous and volatile species during the irradiation of uranium dioxide," *Journal of Nuclear Materials*, vol. 107, pp. 168–184, 6 1982.

[17] C. McKinney, R. Seibert, J. Werden, C. Parish, T. Gerczak, J. Harp, and N. Capps, "Characterization of the radial microstructural evolution in LWR UO_2 using electron backscatter diffraction," *Journal of Nuclear Materials*, vol. 585, p. 154605, 11 2023.

[18] M. Flanagan and P. Askeljung, "Observations of fuel fragmentation, mobility and release in integral high-burnup, fueled LOCA tests," in *Enlarged Halden Program Group Meeting 2011*, 2011.

[19] M. Helin and J. Flygare, "NRC LOCA tests at Studsvik, design and construction of test train device and tests with unirradiated cladding material," Tech. Rep. STUDSVIK/N-11/130, Studsvik, 2012.

[20] G. Pastore, L. Luzzi, V. D. Marcello, and P. V. Uffelen, "Physics-based modelling of fission gas swelling and release in UO_2 applied to integral fuel rod analysis," *Nuclear Engineering and Design*, vol. 256, pp. 75–86, 3 2013.

[21] J. Rest, M. W. Cooper, J. Spino, J. A. Turnbull, P. V. Uffelen, and C. T. Walker, "Fission gas release from UO_2 nuclear fuel: A review," *Journal of Nuclear Materials*, vol. 513, pp. 310–345, 1 2019.

[22] M. Tonks, D. Andersson, R. Devanathan, R. Dubourg, A. El-Azab, M. Freyss, F. Iglesias, K. Kulacsy, G. Pastore, S. R. Phillpot, and M. Welland, "Unit mechanisms of fission gas release: Current understanding and future needs," *Journal of Nuclear Materials*, vol. 504, pp. 300–317, 6 2018.

[23] R. L. Williamson, J. D. Hales, S. R. Novascone, G. Pastore, K. A. Gamble, B. W. Spencer, W. Jiang, S. A. Pitts, A. Casagranda, D. Schwen, A. X. Zabriskie, A. Toptan, R. Gardner, C. Matthews, W. Liu, and H. Chen, "BISON: A flexible code for advanced simulation of the performance of multiple nuclear forms," *Nuclear Technology*, 2021.

[24] G. Pastore, L. P. Swiler, J. D. Hales, S. R. Novascone, D. M. Perez, B. W. Spencer, L. Luzzi, P. V. Uffelen, and R. L. Williamson, "Uncertainty and sensitivity analysis of fission gas behavior in engineering-scale fuel modeling," *Journal of Nuclear Materials*, vol. 456, pp. 398–408, 1 2015.

[25] G. Pastore, D. Pizzocri, C. Rabiti, T. Barani, P. V. Uffelen, and L. Luzzi, "An effective numerical algorithm for intra-granular fission gas release during non-equilibrium trapping and resolution," *Journal of Nuclear Materials*, vol. 509, pp. 687–699, 10 2018.

[26] T. Barani, G. Pastore, A. Magni, D. Pizzocri, P. V. Uffelen, and L. Luzzi, "Modeling intra-granular fission gas bubble evolution and coarsening in uranium dioxide during in-pile transients," *Journal of Nuclear Materials*, vol. 538, p. 152195, 9 2020.

[27] T. Barani, G. Pastore, D. Pizzocri, D. A. Andersson, C. Matthews, A. Alfonsi, K. A. Gamble, P. V. Uffelen, L. Luzzi, and J. D. Hales, "Multiscale modeling of fission gas behavior in U_3Si_2 under LWR conditions," *Journal of Nuclear Materials*, vol. 522, pp. 97–110, 8 2019.

[28] D. Pizzocri, C. Rabiti, L. Luzzi, T. Barani, P. V. Uffelen, and G. Pastore, "Polypole-1: An accurate numerical algorithm for intra-granular fission gas release," *Journal of Nuclear Materials*, vol. 478, pp. 333–342, 9 2016.

[29] D. Pizzocri, G. Pastore, T. Barani, A. Magni, L. Luzzi, P. V. Uffelen, S. A. Pitts, A. Alfonsi, and J. D. Hales, "A model describing intra-granular fission gas behaviour in oxide fuel for advanced engineering tools," *Journal of Nuclear Materials*, vol. 502, pp. 323–330, 4 2018.

[30] T. Barani, E. Bruschi, D. Pizzocri, G. Pastore, P. V. Uffelen, R. L. Williamson, and L. Luzzi, "Analysis of transient fission gas behaviour in oxide fuel using BISON and TRANSURANUS," *Journal of Nuclear Materials*, vol. 486, pp. 96–110, 4 2017.

[31] D. A. Andersson, P. Garcia, X. Y. Liu, G. Pastore, M. Tonks, P. Millett, B. Dorado, D. R. Gaston, D. Andrs, R. L. Williamson, R. C. Martineau, B. P. Uberuaga, and C. R. Stanek, "Atomistic modeling of intrinsic and radiation-enhanced fission gas (Xe) diffusion in $UO_{2\pm x}$: Implications for nuclear fuel performance modeling," *Journal of Nuclear Materials*, vol. 451, pp. 225–242, 8 2014.

[32] A. D. Andersson, "Density functional theory calculations of defect and fission gas properties in u-si fuels," tech. rep., Los Alamos National Laboratory (LANL), LA-UR-15-27996, 2 2016.

[33] N. Capps, L. Aagesen, D. Andersson, O. Baldwin, W. C. Brinkley, M. W. Cooper, J. Harp, S. Novascone, P. C. A. Simon, C. Matthews, and B. D. Wirth, "Empirical and mechanistic transient fission gas release model for high-burnup LOCA conditions," *Journal of Nuclear Materials*, vol. 584, p. 154557, 10 2023.

[34] J. Noirot, I. Zacharie-Aubrun, and T. Blay, "Focused ion beam–scanning electron microscope examination of high burn-up uo2 in the center of a pellet," *Nuclear Engineering and Technology*, vol. 50, pp. 259–267, 3 2018.

[35] L. Yang and B. D. Wirth, "An improved xenon equation of state for nanobubbles in UO_2," *Journal of Nuclear Materials*, vol. 572, p. 154089, 12 2022.

[36] M. W. Cooper, C. Matthews, and D. A. Andersson, "Demonstration of LLS informed fission gas bubble evolution model with micro-cracking for UO_2 in BISON," tech. rep., Los Alamos National Laboratory LA-UR-24-24446, 8 2024.

[37] M. W. Cooper, C. Matthews, and D. A. Andersson, "The role of irradiation-enhanced interstitial diffusion in over-pressurizing fission gas bubbles in UO_2," *Journal of Nuclear Materials, under review*, 2024.

[38] G. Pastore, D. Pizzocri, J. Hales, S. Novascone, D. Perez, B. Spencer, R. Williamson, P. V. Uffelen, and L. Luzzi, "Modelling of transient fission gas behaviour in oxide fuel and application to the BISON code," in *Proceedings of the Enlarged Halden Program Group Meeting. Paper N° F7.4. JRC90392*, OECD Halden Reactor Project, 2014.

[39] K. Lassmann, C. T. Walker, J. van de Laar, and F. Lindström, "Modelling the high burnup UO_2 structure in LWR fuel," *Journal of Nuclear Materials*, vol. 226, pp. 1–8, 10 1995.

[40] T. Barani, D. Pizzocri, F. Cappia, G. Pastore, L. Luzzi, and P. V. Uffelen, "Modeling high burnup structure in oxide fuels for application to fuel performance codes. Part II: Porosity evolution," *Journal of Nuclear Materials*, vol. 563, p. 153627, 5 2022.

[41] M. S. Veshchunov and V. I. Tarasov, "Modelling of irradiated UO_2 fuel behaviour under transient conditions," *Journal of Nuclear Materials*, vol. 437, pp. 250–260, 6 2013.

[42] U. Gösele, "Concentration dependence of rate constants for diffusion- or reaction-controlled void-point-defect reactions," *Journal of Nuclear Materials*, vol. 78, pp. 83–95, 11 1978.

[43] D. Pizzocri, T. Barani, and L. Luzzi, "Sciantix: A new open source multi-scale code for fission gas behaviour modelling designed for nuclear fuel performance codes," *Journal of Nuclear Materials*, vol. 532, p. 152042, 4 2020.

[44] G. Zullo, D. Pizzocri, and L. Luzzi, "The sciantix code for fission gas behaviour: Status, upgrades, separate-effect validation, and future developments," *Journal of Nuclear Materials*, vol. 587, p. 154744, 12 2023.

[45] L. K. A. Jr, S. Biswas, K. A. Gamble, W. Jiang, P.-C. A. Simon, and B. W. Spencer, "Implementation and testing of physics-based pulverization model in BISON," tech. rep., Idaho National Laboratory, 9 2022.

[46] R. J. White and M. O. Tucker, "A new fission-gas release model," *Journal of Nuclear Materials*, vol. 118, pp. 1–38, 8 1983.

[47] R. White, "A new mechanistic model for the calculation of fission gas release," in *Proc. Int. Topical Meeting on LWR Fuel Performance*, p. 196, 1994.

[48] "Scientific issues in fuel behaviour," tech. rep., OECD NEA Nuclear Science Committee Task Force, January 1995.

[49] A. Denis and R. Piotrkowski, "Simulation of isothermal fission gas release," *Journal of Nuclear Materials*, vol. 229, pp. 149–154, April 1996.

[50] L. Bernard and E. Bonnaud, "Finite volume method for fission gas release modeling," *Journal of Nuclear Materials*, vol. 244, pp. 75–84, March 1997.

[51] P. Lösönen, "On the behaviour of intragranular fission gas in UO_2 fuel," *Journal of Nuclear Materials*, vol. 280, pp. 56–72, 6 2000.

[52] C. Walker, P. Knappik, and M. Mogensen, "Concerning the development of grain face bubbles and fission gas release in UO_2 fuel," *Journal of Nuclear Materials*, vol. 160, pp. 10–23, November 1988.

[53] C. Walker and M. Mogensen, "On the rate determining step in fission gas release from high burn-up water reactor fuel during power transients," *Journal of Nuclear Materials*, vol. 149, pp. 121–131, July 1987.

[54] K. Une and S. Kashibe, "Fission Gas Release during Post Irradiation Annealing of BWR Fuels," *Journal of Nuclear Science and Technology*, vol. 42, pp. 1002–1016, May 1990.

[55] M. Mogensen, C. Bagger, and C. Walker, "An experimental study of the distribution of retained xenon in transient-tested UO_2 fuel," *Journal of Nuclear Materials*, vol. 199, pp. 85–101, January 1993.

[56] K. Govers, S. Lemehov, and M. Verwerft, "On the solution and migration of single Xe atoms in uranium dioxide – an interatomic potential study," *Journal of Nuclear Materials*, vol. 405, pp. 252–260, October 2010.

[57] K. Govers, S. Lemehov, and M. Verwerft, "Comparison of interatomic potentials for UO_2. Part I: Static calculations," *Journal of Nuclear Materials*, vol. 366, pp. 161–177, January 2007.

[58] M. Cunningham, M. Freshley, and D. Lanning, "Development and characteristics of the rim region in high burnup UO_2 fuel pellets," *Journal of Nuclear Materials*, vol. 188, pp. 19–27, 1992.

[59] R. Manzel and C. Walker, "EPMA and SEM of fuel samples from PWR rods with an average burn-up of around 100 MWd/kgHM," *Journal of Nuclear Materials*, vol. 201, no. 2-3, pp. 170–182, 2002.

[60] K. Une, K. Nogita, S. Kashibe, T. Toyonaga, and M. Amaya, "Effect of irradiation-induced microstructural evolution on high burnup fuel behaviour," in *Proc. ANS Topical Meeting on Light Water Reactor Fuel Performance*, pp. 478–489, March 2-6 1997.

[61] A. Kolmogorov, "On the Statistical Theory of Metal Crystallization," *Izv. Akad. Nauk SSSR, Ser. Math*, vol. 1, pp. 335–360, 1937.

[62] L. Holt, A. Schubert, P. V. Uffelen, C. T. Walker, E. Fridman, and T. Sonoda, "Sensitivity study on Xe depletion in the high burn-up structure of UO_2," *Journal of Nuclear Materials*, vol. 452, pp. 166–172, 9 2014.

[63] S. Brémier and C. T. Walker, "Radiation-enhanced diffusion and fission gas release from recrystallised grains in high burn-up UO_2 nuclear fuel," *Radiation Effects and Defects in Solids*, vol. 157, pp. 311–322, 2002.

[64] K. A. Gamble, R. T. Sweet, P.-C. A. Simon, L. K. A. Aagesen, and S. Biswas, "Evaluation of mechanistic and empirical models against existing FFRD and LOCA experimental databases," tech. rep., Idaho National Laboratory, INL/RPT-22-69625, 9 2022.

[65] N. Capps, L. Aagesen, D. Andersson, O. B. andW. Cade Brinkley, M. Cooper, J. Harp, S. Novascone, P.-C. A. Simon, C. Matthews, and B. D. Wirth, "Empirical and Mechanistic Transient Fission Gas Release Model for High-Burnup LOCA Conditions," in *Proceedings of the Reactor Fuel Performance Meeting - Top Fuel, under review*, 9 2024.

[66] L. Giaccardi, C. Aguado, I. Guénot-Delahaie, A. Dethioux, J. Zhang, P.-C. A. Simon, and M. Bales, "OECD/NEA Burst Fission Gas Release Benchmark Based on REGATE and HATAC-C2 Tests," in *Proceedings of the Reactor Fuel Performance Meeting - Top Fuel, under review*, 9 2024.

[67] S. Djurle, "Final Report of the Super-Ramp Project," Tech. Rep. STSR-32, Studsvik Energiteknik, AB, 1984.

[68] E. Sartori, J. Turnbull, and J. Killeen, "Nuclear energy agency (nea) - international fuel performance experiments (ifpe) database," 2010.

[69] M. E. Flanagan, P. Askeljung, and A. Puranen, "Evaluation of Mechanistic and Empirical Models against Existing FFRD and LOCA Experimental Databases," Tech. Rep. NUREG-2160, United States Nuclear Regulatory Commission, 2013.